Interstellar Seeing. I. Superresolution Techniques Using Radio Scintillations

J. M. Cordes
Astronomy Department, 520 Space Sciences Building, Cornell University, Ithaca, NY 14853
cordes@spacenet.tn.cornell.edu

Submitted to *Astrophysical Journal* **July 19, 2000**

ABSTRACT

Interstellar scintillation can be used to probe transverse sizes of radio sources on scales inaccessible to the nominal resolution of any terrestrial telescope, e.g. $\lesssim 10^{-6}$ arc sec. Methodology is presented that exploits this superresolution phenomenon for both single aperture and interferometer observations. The treatment applies to the saturated (strong-scattering) regime and holds for both thin screens and extended media. A general signal model for radio sources is presented, *scintillated amplitude modulated noise*, which applies to compact, incoherent synchrotron sources such as AGNs and gamma-ray burst sources and also to known, coherent sources such as masers and pulsars. The exact probability density function for measured intensities and interferometric visibilities is obtained by solving a general Fredholm problem. An approximate density function is also obtained by using the equivalent number of degrees of freedom in scintillation modulations. The scintillation modulation variance is presented, which includes the effects of source structure and time-bandwidth averaging in the signal processing. Two Bayesian methods are outlined for inferring the sizes of emission regions that use first order statistics of the intensity and visibility. Intensity cross-correlation methods for inferring source sizes are also given. Intensity interferometry in the the radio context is compared to the optical intensity interferometry of Hanbury-Brown and Twiss.

1. Introduction

Diffractive interstellar scintillation (DISS) is caused by multipath scattering of radio waves from small-scale density irregularities in the ionized interstellar medium. It is sensitive to intrinsic sizes of radiation sources in much the same way that optical scintillation from atmospheric turbulence is quenched for planets while strong for stars. However, interstellar scintillation differs from the atmospheric case in that it can resolve sources at angular resolutions much smaller than those achievable with available apertures, including the longest baselines used in very long baseline interferometry (VLBI), those using space antennas. Optical techniques such as intensity interferometry, speckle interferometry and adaptive optics typically only *restore* the telescope resolution to what it would be in the absence of any atmospheric turbulence.

We define the *superresolution regime* where the source is unresolved by terrestrial interferometers but is sufficiently extended to modify the DISS. Let θ_s, θ_{ij} and θ_{iso} be the source size, interferometer fringe spacing, and isoplanatic DISS patch, respectively. By definition, two point sources separated by much less than the isoplanatic angle will show identical DISS. The isoplanatic angle $\theta_{iso} \sim \lambda/d\theta_d$, where λ is the wavelength, θ_d is the size of the scattering ("seeing") disk and d is the source-Earth distance. Using typical numbers ($d = 1$ kpc, $\theta_d = 1$ mas at an observing frequency of 1 GHz), $\theta_{iso} \sim 0.4\,\mu$arc sec. For pulsars, whose light-cylinder radii, $r_{\rm LC} = cP/2\pi$ (P = spin period) are smaller than 1 μarc sec at typical distances, we have $\theta_{iso} \lesssim \theta_s \ll \theta_{ij}$ and $\theta_{iso} \ll \theta_d$. In this case, speckle methods can achieve far better resolution than the interferometer. By speckle methods, we mean observations that analyze differences in the DISS between source components, which are sensitive to the spatial separations of those components. Cornwell & Narayan (1993) have discussed particular superresolution techniques in the radio context. In optical astronomy, superresolution is not achievable because $\theta_d \sim \theta_{iso}$. However, the superresolution regime has been identified in optical laboratory applications (Charnotskii, Myakinin & Zavorotnyy 1990).

The purpose of this paper is to provide a rigorous and general formulation of DISS that can be used in superresolution applications. Previous work has relied on DISS theories that are restricted to particular spatial geometries (e.g. thin screens) or to particular wavenumber spectra (e.g. a power law with the "Kolmogorov" slope.). In subsequent papers, we will apply the methods of this paper to scintillation observations and derive constraints on pulsar source sizes.

Our treatment builds upon work published in both the optical and radio propagation literature and is unique in the following ways: (1) it interfaces empirical astrophysical constraints on source radiation fields with the scattering geometry and scattering strength appropriate for radio observations; (2) it calculates fluctuation statistics of realistically measureable quantities in single-aperture and interferometric observations, taking into account all sources of fluctuation; (3) we present exact calculations for the intensity probability density function (PDF) that take into account arbitrary source brightness distributions and arbitrary amounts of time-bandwidth averaging; and (4) our results can be applied to a wide range of media with arbitrary spatial extent and wavenumber spectrum. Gwinn *et al.* (1998) discuss issues that are very similar to those contained in this paper. Our treatment is more general than Gwinn *et al.*'s because it is not limited to scattering media contained in thin screens. Also, our treatment of the probability distribution is not restricted to small source sizes (compared to the isoplanatic scale). Finally, our treatment includes the effects of intrinsic source fluctuations, which are assumed negligible by Gwinn *et al.*

We restrict the analysis to strong (saturated) DISS. Another component — refractive interstellar scintillations (RISS) — also modulates source intensitities, but on time scales much longer than for DISS. RISS can be seen from larger angular diameter sources, by a factor of 1000, than can DISS. We are interested in modeling data spans much shorter than the characteristic RISS time scale, so we ignore RISS in our discussion. The cases we consider are what would be

called the "single speckle" regime in the optical literature. This corresponds to the case where the aperture size (either a single dish diameter or an interferometer baseline) is smaller than the diffraction length scale (e.g. the Fried scale). However, our formalism can be extended easily to include aperture averaging and multiple speckle cases.

In §2 we briefly summarize previous work on use of DISS to resolve radio sources. In §3 we present a general signal model and in §4 give expressions for the modulation index of the interferometric visibility and single aperture intensity. We take into account time-bandwidth averaging and source extent. We calculate an approximate PDF of the visibility and intensity using the number of degrees of freedom in the scintillations. We also outline the exact calculation of the PDF. §5 presents a Bayesian inference method for the source size. The paper is summarized in §6. The details of our definitions and calculations are given in three Appendices. In Appendix A we derive the statistics and scintillations of the scintillating amplitude modulated noise model. In Appendix B we derive second moments for the intensity and visiblity. In Appendix C we derive the PDFs for the scintillations, total intensity, and visiblity.

Notation required in discussions of wave propagation through random media is necessarily copious. Apart from standard definitions for wavelength, frequency, speed of light, and wavenumber (λ, ν, c and $k = 2\pi/\lambda$, we list in Table 1 those symbols that are used throughout the paper.

2. Previous Applications of DISS Superresolution

DISS superresolution techniques have been used in several ways to probe source structure. DISS has been sought from various kinds of AGNs (Condon & Backer 1975; Armstrong, Spangler & Hardee 1977; Condon & Dennison 1978; Dennison & Condon 1981), leading to bounds on the brightness temperature and limits on the Lorentz factors of bulk relativistic flow. Lovelace (1970) first suggested that DISS might resolve pulsar magnetospheres. Backer (1975) placed coarse limits on the sizes of pulsar magnetospheres by considering the fractional modulation of DISS for a few pulsars. Cordes, Weisberg & Boriakoff (1983; hereafter CWB83) placed upper bounds on the source extent, and emission altitude, for two pulsars, finding upper bounds on emission altitudes of $0.5r_{\rm LC}$ and $0.1r_{\rm LC}$. Wolszczan & Cordes (1987) exploited a remarkable episode of multiple imaging of a pulsar by a refracting interstellar structure; they found that (a) different pulse components from a long-period pulsar showed nonidentical DISS, signifying source resolution; and (b) the implied emission altitude is comparable to $r_{\rm LC}$, in contrast to other estimates, based on pulse widths and polarization, which suggest emission altitudes of only 1-10% of $r_{\rm LC}$ (Blaskiewicz *et al.* 1991). Kuzmin (1992) and Smirnova, Shishov & Malofeev (1996) reported similar results on four additional long-period pulsars, again with implied emission radii $\sim r_{\rm LC}$.

Recently, Gwinn *et al.* (1997,2000) have analyzed VLBI observations of the Vela pulsar using time and frequency resolutions that exploit the same spatial resolving power of DISS as do the single-dish observations used by others. Through estimation of the probability density function

(PDF) of the visibility function magnitude, they infer that DISS shows less modulation than expected from a point source and therefore conclude that the source must be extended. They estimate a transverse size $\sim$ 500 km for the region responsible for the pulsed flux in a narrow range of pulse phase.

In a second paper, we reassess the conclusions of Gwinn *et al.* (1997) by considering how time-frequency averaging in the signal processing affects inferences on source size from visibility fluctuations. Gwinn *et al.* (1999) have also considered time-frequency averaging and the effects of source fluctuations. The approaches differ and yield different conclusions about the importance of averaging and source noise as well as differing on estimates of the source size.

Also recently, radio observations of gamma-ray burst (GRB) afterglows suggest that DISS occurs in the early stages and then is quenched as expanding synchrotron sources are first smaller than, and then exceed, the isoplanatic scale (Goodman 1997; Frail *et al.* 1997). If GRB synchrotron sources are incoherent sources, the angular size requirements for DISS to appear are severe. We defer to another paper a discussion of GRB scintillation.

3. Signal Model for Scintillating Sources

To account for all contributions to measureable quantities, we need a comprehensive statistical model for the received signal. The model presented here includes a source that is temporally incoherent but has arbitrary spatial coherence; diffractive interstellar scintillation from an arbitrary distribution of scattering material along the line of sight; and additive radiometer noise.

We define $\varepsilon(\mathbf{r}, t)$ to be the complex, narrowband, baseband scalar electric field that is explicitly or implicitly manipulated in radio astronomy systems. (For definitions, see Appendix A.) It is determined by the source emission mechanism and by propagation effects through intervening media, as well as by receiver and background sky noise. We consider source emission that has underlying Gaussian statistics and propagation effects from the turbulent, ionized interstellar medium (ISM). The field measured at position $\mathbf{r}$ is the superposition of scintillating source components and radiometer noise, $n(\mathbf{r}, t)$,

$$\varepsilon(\mathbf{r}, t) = \int d\mathbf{r_s}\, \varepsilon_s(\mathbf{r_s}, t) g(\mathbf{r}, t, \nu, \mathbf{r_s}) + n(\mathbf{r}, t). \tag{1}$$

All vectors are two-dimensional and transverse to the line of sight. The corresponding intensity is

$$I(\mathbf{r}, t) = |\varepsilon(\mathbf{r}, t)|^2. \tag{2}$$

The quantity $\varepsilon_s(\mathbf{r}, t)$ is the field emitted per unit area at the source but whose amplitude includes implicitly an inverse distance dependence. Propagation is described by the quantity $g(\mathbf{r}, t, \nu, \mathbf{r_s})$, which is the propagator for a point source at location $\mathbf{r_s}$. It includes a phase factor

for free-space propagation as well as phase and amplitude factors associated with DISS.[1] Here ν is the center frequency of the passband with bandwidth $\Delta\nu$ that is selected by the receiver and mixed to baseband. The notation for $\varepsilon(\mathbf{r},t)$ and $n(\mathbf{r},t)$ leaves this center frequency implicit; but each of these quantities is a time series of a narrowband process and is the baseband equivalent of the narrowband radiation field selected by the receiver. Further justification for this model is given in Appendix A.

The field emitted by the source is taken to be amplitude modulated noise (Rickett 1975; Cordes 1976b), $\varepsilon_s(\mathbf{r_s},t) = a(\mathbf{r_s},t)m(\mathbf{r_s},t)$, which is a physically motivated and empirically confirmed model for most astrophysical sources. The amplitude modulated noise model includes nonstationary modulations $a(\mathbf{r_s},t)$ of stationary noise $m(\mathbf{r_s},t)$. The noise correlation function is $\langle m(\mathbf{r_{s1}},t_1)m^*(\mathbf{r_{s2}},t_2)\rangle = \delta(\mathbf{r_{s2}}-\mathbf{r_{s1}})\Delta(t_2-t_1)$, where the asterisk denotes complex conjugation, angular brackets denote ensemble average, and $\Delta(\tau)$ is a continuous delta-function-like quantity with $\Delta(0)=1$ and width equal to the reciprocal bandwidth of the receiving system. The additive noise, $n(\mathbf{r},t)$, also is 'Δ' correlated in time and is assumed spatially uncorrelated across nonzero baselines, $\mathbf{b}=\mathbf{r}_2-\mathbf{r}_1$.

3.1. Interferometer Visibility Function & Phase Structure Function

It is well known that the mean visibility function of a scattered point source (in strong scattering) is the product of the true source visibility $\Gamma_s(\mathbf{b})$ and the second moment of the DISS modulation, $\gamma_{\rm g}$ (e.g. Rickett 1990 and references therein):

$$\langle\Gamma_\varepsilon(\mathbf{b},\tau_i)\rangle = \langle\varepsilon(\mathbf{r},t)\varepsilon^*(\mathbf{r}+\mathbf{b},t+\tau_i)\rangle = \Delta(\tau_i)\gamma_{\rm g}(\mathbf{b},0,0,0)\Gamma_s(\mathbf{b}). \tag{3}$$

The source visibility is the usual Fourier transform of the brightness distribution, $I_s(\mathbf{r_s}) = A(\mathbf{r_s}) = a^2(\mathbf{r_s})$,

$$\Gamma_s(\mathbf{b}) = \int d\mathbf{r_s}\, e^{+ikd^{-1}\mathbf{r_s}\cdot\mathbf{b}} I_s(\mathbf{r_s}), \tag{4}$$

where d is the source-observer distance and $k = 2\pi c^{-1}\nu$. We use a spatial vector, $\mathbf{r_s}$, to define the source brightness distribution rather than using an angular variable, as is common practice. We assume that the propagation delay between the pair of sites has already been removed, so the visibility function maximizes at $\tau_i \lesssim (\Delta\nu)^{-1}$.

---

[1]The form of Eq. 1 is approximate. Factoring the integrand relies on ε_s being narrowband with bandwidth $\Delta\nu \ll \nu$, that it varies much faster than the DISS propagator, g, and that the bandwidth is much smaller than the characteristic scintillation bandwidth, i.e. the characteristic bandwidth on which g changes. This last constraint is identical to requiring that differential propagation times be much less than the shortest characteristic time scale of the signal. Later, we also consider variations of g with frequency. The signal model presented still applies if we consider the total frequency range to comprise many separate intervals in each of which g is piecewise constant.

The factor $\gamma_{\rm g}$ in Eq. 3 is proportional to the second cross moment of the propagator, $g(\mathbf{r}, t, \nu, \mathbf{r_s})$, at two observation positions, times and frequencies separated by $\mathbf{b}$, τ, $\delta\nu$, respectively, and for two point sources separated by $\delta\mathbf{r_s}$:

$$\Gamma_g(\mathbf{b}, \tau, \delta\nu, \delta\mathbf{r_s}) \quad = \quad \langle g(\mathbf{r}, t, \nu, \mathbf{r_s}) g^*(\mathbf{r}+\mathbf{b}, t+\tau, \nu+\delta\nu, \mathbf{r_s}+\delta\mathbf{r_s})\rangle = e^{-i\psi}\gamma_{\rm g}(\mathbf{b}, \tau, \delta\nu, \delta\mathbf{r_s}). \quad (5)$$

In this equation, the phase ψ is determined by free-space propagation and drops out in much of what appears below, but is responsible for the Fourier relation in Eq. 4. Appendix A shows the details. The form for $\gamma_{\rm g}$ with zero frequency lag ($\delta\nu = 0$) is simply expressed in the Gaussian limit using the phase structure function, $D_\phi(\mathbf{b}, \tau, \delta\mathbf{r_s})$,

$$\gamma_{\rm g}(\mathbf{b}, \tau, \delta\nu = 0, \delta\mathbf{r_s}) \quad = \quad e^{-\frac{1}{2}D_\phi(\mathbf{b}, \tau, \delta\mathbf{r_s})}. \quad (6)$$

For nonzero frequency lags, a closed-form expression for $\gamma_{\rm g}$ is not usually available. The DISS "gain" $G = |g|^2$, has unit mean, $\langle G\rangle = 1$, and has a normalized autocovariance in the strong scattering (Rayleigh) limit,

$$\gamma_{\rm G}(\mathbf{b}, \tau, \delta\nu, \delta\mathbf{r_s}) = \langle G(\mathbf{r}, t, \nu, \mathbf{r_s}) G(\mathbf{r}+\mathbf{b}, t+\tau, \nu+\delta\nu, \mathbf{r_s}+\delta\mathbf{r_s})\rangle - 1 = |\gamma_{\rm g}(\mathbf{b}, \tau, \delta\nu, \delta\mathbf{r_s})|^2. \quad (7)$$

For a medium in which scattering occurs with variable strength all along the line of sight, the phase structure function is (Lotova & Chashei 1981; Cordes & Rickett 1998)

$$D_\phi(\mathbf{b}, \tau, \delta\mathbf{r_s}) \quad \propto \quad \lambda^2 \int_0^d ds\, C_n^2(s)\, |\mathbf{b}_{\rm eff}(s)|^\alpha \quad (8)$$

$$\mathbf{b}_{\rm eff}(s) \quad = \quad (s/d)\mathbf{b} + \mathbf{V}_{\rm eff}(s)\tau + (1-s/d)\delta\mathbf{r_s} \quad (9)$$

$$\mathbf{V}_{\rm eff}(s) \quad = \quad (s/d)\mathbf{V}_{\rm obs} + (1-s/d)\mathbf{V}_{\rm p} - \mathbf{V}_{\rm m}(s). \quad (10)$$

C_n^2 is the coefficient in the wavenumber spectrum for electron density variations and α is the exponent of the structure function. For a square-law structure function $\alpha = 2$, while for a Kolmogorov medium in strong, but not superstrong scattering (Cordes & Lazio 1991), $\alpha = 5/3$. $\mathbf{V}_{\rm p}$ is the pulsar velocity, $\mathbf{V}_{\rm obs}$ is the observer's velocity and $\mathbf{V}_{\rm m}$ is the velocity of the scattering material in the ISM. For the case $C_n^2(s) \propto \delta(s - D_s)$, where D_s is the distance of a scattering screen from a pulsar, we retrieve the result applicable for a thin-screen.

Note that the phase structure function $\propto \lambda^2$ for radio propagation through tenuous plasmas. For optical and infrared (IR) propagation through the atmosphere, $D_\phi \propto \lambda^{-2}$.

Our expressions Eq. 7-10 are quite general, being based on Gaussian statistics for the wavefield and on the saturated (Rayleigh) regime of scattering. As such, they can be used for observations of Galactic and extragalactic radio sources, including pulsars, masers, microquasars, active-galactic nuclei, and gamma-ray burst sources.

Our form for D_ϕ applies to isotropic scattering irregularities. Evidence exists for anisotropies in heavily scattered sources (Frail *et al.* 1994; Wilkinson, Narayan & Spencer 1994; Yusef-Zadeh 1994; Molnar *et al.* 1995; Desai & Gwinn 1998; Spangler & Cordes 1998; Trotter, Moran & Rodriguez 1998). Though, for simplicity, we consider only the isotropic case in this paper, it is a simple matter to extend our results to the anisotropic case, which we will do elsewhere.

3.2. Isoplanatic Scales

DISS is correlated over spatial and temporal scales at the observer's location that are determined by contours of constant D_ϕ. For a thin screen at $s = D_s$ from the source, we write $D_\phi = (|\mathbf{b}_{\rm eff}|/b_e)^\alpha$, with $\mathbf{b}_{\rm eff}$ given by Eq. 9 and where b_e is the 1/e scale of the structure function. We define the isoplanatic length scale and time scale through $D_\phi(\mathrm{b_{iso}}, 0, 0) = 1$ and $D_\phi(0, \Delta t_{\rm d}, 0) = 1$, yielding $b_{iso} = b_e(d/D_s)$ and, if the source's speed dominates $\mathrm{V_{eff}}$ (as it does for many pulsars), $\Delta t_{\rm d} = b_e/(1 - D_s/d)V_{\rm p}$. We also define the isoplanatic scale at the source's location using $D_\phi(0, 0, \delta\mathbf{r_{s,iso}}) = 1$, resulting in $\delta r_{s,iso} = b_e(1 - D_s/d)^{-1} = V_{\rm p}\Delta t_{\rm d}$. The isoplanatic scale $\delta r_{s,iso}$ defines the separation at which two point sources would scintillate with a correlation coefficient of e^{-1}. This scale determines whether DISS can resolve a source, as discussed in the Introduction. For reference, the Fried scale r_0, defined in the optical and IR literature, is related to our definitions using $D_\phi(b, 0, 0) = 6.88(b/r_0)^{5/3}$ (e.g. Goodman 1985), so $r_0 \approx 3.2b_e$. Also, in the radio case $r_0 \propto \lambda^{-6/5}$ while $r_0 \propto \lambda^{+6/5}$ for optical/IR propagation.

In strong scattering, the isoplanatic scale is smaller, in some cases by three orders of magnitude or more, than the Fresnel scale. The Fresnel scale, at meter wavelengths, $\sim \sqrt{\lambda D} \approx 10^{11}$ cm for kiloparsec distances.

The isoplanatic scale $\delta r_{s,iso}$ is smaller for sources that are scattered more heavily. This corresponds to more distant sources, sources viewed through regions of excess scattering, or sources observed at longer wavelengths. For a continuous source, such as one with a Gaussian brightness distribution, its size compared to $\delta r_{s,iso}$ determines the depth of modulation of the DISS. To apply this basic idea, however, averaging over time and over the receiver bandwidth must also be dealt with carefully because it too affects the depth of modulation. We now consider all these effects in what follows.

4. Resolving Sources with Scintillations

Several methods can be used to exploit the scintillation phenomenon in order to resolve sources. These are (1) measurement of the fractional modulation of the source through analysis of the intensity variance; (2) estimation of the intensity PDF, equivalent to analysis of *all* moments; and (3) use of cross-correlation functions for the DISS of separate sources to measure the spatial offsets of those sources.

4.1. Visibility and Intensity Statistics

The visibility function and the intensity are both second field moments. Estimates of these second moments from finite data sets fluctuate by amounts that are formally described by the fourth field moment. Encoded in these fluctuations is information about source structure and

the intervening medium. We use a normalized fourth moment — a generalized modulation index (squared) — to cast intensity and visibility fluctuations in a similar form. The modulation index includes the effects of averaging over time and frequency and is calculated for an arbitrary source brightness distribution.

4.2. Autocorrelation Functions

To model realistic cases, we take into account averaging over time and the finite bandwidth of the narrowband signal. For simplicity, we refer to the finite bandwidth as "frequency averaging.' To resolve DISS, the averaging intervals T and B must be smaller than the characteristic correlation scales of G, the DISS gain in time and frequency. These are usually called the DISS or 'scintillation' time scale and bandwidth, denoted $\Delta t_{\rm d}$ and $\Delta\nu_{\rm d}$, respectively.

Let $\overline{\rm I}(\mathbf{r},t)$ be the intensity at location $\mathbf{r}$ calculated for a narrowband signal with bandwidth B after averaging over the interval $[t-T/2, t+T/2]$. Define also the averaged visibility function as $\overline{\Gamma}(\mathbf{b},t)$, calculated between two sites separated by baseline $\mathbf{b}$ and with time lag τ but with zero frequency lag. The autocorrelation functions (ACFs) of the intensity and visibility are

$$R_{\overline{\rm I}}(\mathbf{b},\overline{\tau}) \equiv \left\langle \overline{\rm I}(\mathbf{r},t)\overline{\rm I}(\mathbf{r}+\mathbf{b},t+\overline{\tau})\right\rangle \tag{11}$$

$$R_{\overline{\Gamma}}(\mathbf{b},\overline{\tau}) \equiv \left\langle \overline{\Gamma}(\mathbf{r},t)\overline{\Gamma}^{*}(\mathbf{r}+\mathbf{b},t+\overline{\tau})\right\rangle \tag{12}$$

4.3. Modulation Indices

To quantify fluctuations of $\overline{\rm I}$ and $\overline{\Gamma}$, we calculate the modulation indices,

$$m^2_{\overline{\rm I}}(\mathbf{b},\tau) \equiv \frac{R_{\overline{\rm I}}(\mathbf{b},\tau) - \langle {\rm I}\rangle^2}{\langle {\rm I}\rangle^2} \tag{13}$$

$$m^2_{\overline{\Gamma}}(\mathbf{b},\tau) \equiv \frac{R_{\overline{\Gamma}}(\mathbf{b},\tau) - |\langle \Gamma_\varepsilon\rangle|^2}{\langle {\rm I}\rangle^2}, \tag{14}$$

where we normalize by the mean intensity in both cases. As shown in Appendix B, the modulation index receives contributions from four terms. For compact sources, the dominant term is in fact caused by DISS and is given by

$$m^2_{\rm ISS}(\mathbf{b},\overline{\tau}) = \langle I\rangle^{-2}\int\int d\mathbf{r}_{\mathbf{s}1}\, d\mathbf{r}_{\mathbf{s}2}\, I_s(\mathbf{r}_{\mathbf{s}1})\, I_s(\mathbf{r}_{\mathbf{s}2})\, Q_{\rm ISS}(\mathbf{b},\overline{\tau},\mathbf{r}_{\mathbf{s}2}-\mathbf{r}_{\mathbf{s}1},T,B), \tag{15}$$

where, for uniform averaging[2] in T and B,

$$Q_{\rm ISS}(\mathbf{b},\overline{\tau},\delta\mathbf{r_s},T,B) = (TB)^{-1}\int_{-T}^{+T} d\tau'\left(1-\left|\frac{\tau'}{T}\right|\right)\int_{-B}^{+B} d\delta\nu\,\left(1-\left|\frac{\delta\nu}{B}\right|\right) \times\begin{cases}\gamma_{\rm G}(\mathbf{b},\tau'+\overline{\tau},\delta\nu,\delta\mathbf{r_s}) & \text{intensity}\\ |\Delta(\tau_i)|^2\,e^{-ikd^{-1}\mathbf{b}\cdot\delta\mathbf{r_s}}\gamma_{\rm G}(0,\tau'+\overline{\tau},\delta\nu,\delta\mathbf{r_s}) & \text{visibility,}\end{cases} \quad (16)$$

with $\gamma_{\rm G}$ defined in Eq. 7. Visibility fluctuations are independent of baseline $\mathbf{b}$ for unresolved sources, for which the complex exponential $\rightarrow 1$, while intensity variations depend more strongly on $\mathbf{b}$, even for sources unresolved by the baseline. The baseline-independent property for visibility fluctuations is similar to the conclusion found by Goodman & Narayan (1989). The difference between intensity and visibility statistics arises from the ordering of the time-averaging and cross-correlation operations in the two cases.

The modulation index, as presented here, includes only DISS fluctuations. There are additional contributions to the visibility or intensity variance from intrinsic source fluctuations and from additive noise. These are secondary to our discussion here, but are important in any practical application where the time-bandwidth product is low and where intrinsic source fluctuations are high. For pulsars, pulse-to-pulse amplitude variations are important when only a few pulses are included in any averaging. Appendix B gives full expressions for all contributions to intensity variations.

4.4. Number of Degrees of Freedom in Fluctuations

TB averaging and extended structure expressed in the integrals of $\gamma_{\rm G}$ in Eq. 15,16 diminish scintillation fluctuations. The modulation index of the averaged intensity or visibility depends on time averaging and source extension in similar ways because both increase the number of degrees of freedom in the integrated intensity. The number of degrees of freedom is

$$N_{\rm dof} = 2m_{\rm ISS}^{-2} = 2N_{\rm ISS} \geq 2, \quad (17)$$

where $N_{\rm ISS}$ is the number of independent DISS fluctuations ("scintles") that are averaged. For observations in the single speckle regime, where scintles are resolved in time and frequency, we expect $1 \leq N_{\rm ISS} \lesssim 2$.

---

[2]Uniform averaging over frequency corresponds to spectrometer passbands that are perfectly rectangular; real passbands, $h(\nu)$, have shapes similar to Gaussian functions and can be handled by replacing $1-|\delta\nu/B|$ in Eq. 16 with the autocorrelation of $h(\nu)$ and extending the limits to $\pm\infty$. Computations show that this refinement produces no significant changes in our discussion.

4.5. Examples

In Figures 1-3 we show $m^2_{\rm ISS}$ plotted against integration time T for different values of bandwidth B. These cases are for a point source. In the figures, we use T and B normalized by the scintillation time scale, $\Delta t_{\rm d}$, and bandwdith, $\Delta\nu_{\rm d}$. Figure 1 is the case for a thin screen with a square-law structure function (i.e. $\alpha = 2$). Figure 2 is for a thin screen with $\alpha = 5/3$, the form appropriate for a Kolmogorov medium if the scattering is strong but not ultrastrong (Cordes & Lazio 1991). Finally, Figure 3 is the Kolmogorov case for an extended medium with uniform statistics along the line of sight.

The differences between the plotted curves for the different media are subtle, but nonetheless significant if one were to use the modulation index (for given T, B, say) to try to determine what kind of medium was responsible for a given measurement. More importantly, the differences must be considered when assessing whether the source is extended.

To consider source-size effects, we adopt a circular Gaussian brightness distribution with source size, σ_r,

$$I_s(\mathbf{r_s}) = \left(2\pi\sigma_r^2\right)^{-1} \exp\left(-\frac{|\mathbf{r_s}|^2}{2\sigma_r^2}\right). \tag{18}$$

For this case, the squared modulation index is

$$m^2_{\rm ISS}(\mathbf{b},\overline{\tau}) \;\; = \;\; (4\pi\sigma_r^2)^{-1} \int d\delta\mathbf{r_s}\, e^{-(|\delta\mathbf{r_s}|/2\sigma_r)^2} Q_{\rm ISS}(\mathbf{b},\overline{\tau},\delta\mathbf{r_s},T,B). \tag{19}$$

Figures 4-6 show $m^2_{\rm ISS}$ plotted against source size in units of the isoplanatic scale, $\delta r_{s,iso}$ (defined in §3.2). The three figures are for the same square-law, thin-screen Kolmogorov, and uniform Kolmogorov media considered in Figures 1-3, which are results for point sources. The different curves are for different combinations of $T/\Delta t_{\rm d}$ and $B/\Delta\nu_{\rm d}$. One feature to note is that $m^2_{\rm ISS}$ falls off more rapidly with source size $\sigma_r/\delta r_{s,iso}$ than it does with $T/\Delta t_{\rm d}$ or with $B/\Delta\nu_{\rm d}$. This is because the source-size dependence results from a two-dimensional integration over the difference vector $\mathbf{r_{s2}} - \mathbf{r_{s1}}$ in Eq. 15 as compared with one-dimensional integrals for TB averaging. These figures show again that any inference on source size must account not only for TB-averaging, but also for the type of medium underlying the measurements. Furthermore, the predicted contributions from TB-averaging rely on accurate measurements of the DISS time scale and bandwidth.

4.6. Interpretation of Modulation Index

Application of Eq. 15 is as follows. If $m^2_{\rm ISS} = 1$ (within errors) then the source is unresolved by the DISS, the baseline $\mathbf{b}$ has not resolved the scattering disk, *and* the scintillations cannot have

decorrelated over the averaging intervals T and B. The DISS gain G then has an exponential PDF associated with the two degrees of freedom in the scattered wavefield.

Alternatively, $m_{\rm ISS}^2 < 1$ can signify (1) resolution of the scattering disk by the baseline (in the case of intensity interferometry); (2) variation of the DISS over the averaging time or averaging bandwidth; *or* that (3) the source has been resolved by the DISS, i.e. that it is comparable to or larger than the isoplanatic scale of the DISS. To discriminate between these possibilities, auxiliary information is needed that characterizes the dependence of $\gamma_{\rm g}$ on its four arguments, $\mathbf{b}, \tau, \delta\nu$, and $\delta\mathbf{r_s}$. Such information is obtained by making DISS and angular broadening measurements over a wide range of frequencies (e.g. Rickett 1990).

Complications in estimating $m_{\rm ISS}^2$ arise from the fact that scintillating sources fluctuate, on inverse-bandwidth time scales and on a variety of longer time scales, and there is additive noise in any real-world receiver system. We consider all such complications in Appendices B and C and also in the next few sections.

4.7. PDF of the Averaged DISS Gain

While the modulation index of visibility fluctuations may allow inference of source structure, an analysis of the full probability density function (PDF) may be more sensitive. Here we investigate the PDF for several cases.

First consider a scintillating point source with no TB averaging of G. As is well known, the intensity PDF is a one-sided exponential in the limit of no additive noise because G is a chi-square random variable (RV) with two degrees of freedom, χ_2^2 (e.g. Goodman 1985). TB averaging and extended sources increase the number of degrees of freedom, and therefore decrease $m_{\rm ISS}^2$, as discussed in §4.4. If TB averaging and source superposition are viewed as combining statistically independent RV, G is distributed as $\chi_{2N_{\rm ISS}}^2$,

$$f_G(G) \approx \frac{(GN_{\rm ISS})^{N_{\rm ISS}}}{G\Gamma(N_{\rm ISS})} e^{-GN_{\rm ISS}} U(G), \tag{20}$$

where $\Gamma(x)$ is the gamma function and $U(x)$ is the unit step function. In detail, however, the intensity (or visibility) is the integral of variables that are statistically dependent, so the $\chi_{2N_{\rm ISS}}^2$ PDF is only an approximation to the true PDF of G.

The true PDF is calculated by solving a homogeneous Fredholm equation of the second kind (Press *et al.* 1992, pp. 779-785) that results from expanding the propagator $g(\mathbf{r}, t, \mathbf{r_s}, \nu)$ onto an orthonormal set of eigenvectors ψ_n (e.g. Goodman 1985, pp. 250-256) and requiring that the expansion coefficients be statistically independent (a Karhunen-Loève expansion). The general case, where time-bandwidth averaging and source extension must be considered, requires solution

of the eigenvalue problem (see Appendix C)

$$(TB)^{-1}\int_{t-T/2}^{t+T/2}dt'\int_{-B}^{+B}d\delta\nu\,\left(1-\frac{|\delta\nu|}{B}\right)\int d\mathbf{r_{s1}}\,[I_s(\mathbf{r_{s1}})I_s(\mathbf{r_{s2}})]^{1/2}$$
$$\gamma_{\rm g}(0,t''-t',\delta\nu,\mathbf{r_{s2}}-\mathbf{r_{s1}})\psi_n(t',\mathbf{r_{s1}})=\lambda_n\psi_n(t',\mathbf{r_{s2}}), \qquad (21)$$

where the λ_n are the eigenvalues. The time and frequency integrands are slightly different because the wave propagator, g, is integrated over frequency before squaring of the wavefield, while time-averaging occurs after squaring.

For the simple example of a time average of G at discrete times $t_j = j\Delta t$, $j = 1,\ldots,N$, the eigenvectors $\psi_n(t_j)$ and eigenvalues λ_n are solutions of

$$\sum_{i=1}^{N}\gamma_{\rm g}(0,t_i-t_j,0,0)\psi_n(t_i)=\lambda_n\psi_n(t_j),\ n=1,\ldots,N. \qquad (22)$$

The PDF of $G = N^{-1}\sum_i |g(t_i)|^2$ is the N-fold convolution of one-sided exponential PDFs, each of which has mean λ_n/N, because each coefficient b_n in the expansion of $g(t)$ is statistically independent and is a complex, Gaussian RV. The PDF can be written in the form $f_G(G) = \sum_n c_n \exp(-G\,N/\lambda_n)$ where the c_n are functions of the eigenvalues, $c_n = \lambda_n^{-1}\prod_{n'\neq n}(1-\lambda_{n'}/\lambda_n)^{-1}$. Frequency averaging behaves similarly.

Goodman (1985) has shown that exact PDFs calculated in this way are fairly well approximated by the $\chi^2_{2N_{\rm ISS}}$ PDF with the appropriate number of degrees of freedom given by Eq. 17. The approximate PDF has the same mean and variance as the exact PDF. In the limits $N_{\rm ISS} \to 1$ and $N_{\rm ISS} \gg 1$, the two PDFs become identical. Also, if an observable is calculated as the sum of strictly independent DISS fluctuations with equal variances, then the exact PDF is the $\chi^2_{2N_{\rm ISS}}$ PDF.

Figure 7 shows exact PDFs for different instances of time averaging and finite source size. The results are for a Kolmogorov wavenumber spectrum ($\alpha = 5/3$) but do not differ substantially for a square-law structure function. Figure 7a is a sequence of PDFs for time-averaging and for a point source, while Figure 7b is a sequence of PDFs for finite source sizes but with no time-averaging. Also shown in Figure 7c are approximate PDFs based on the χ^2 PDF for different numbers of degrees of freedom given by $2N_{\rm ISS}$, where values of $N_{\rm ISS}$ are chosen to yield PDFs of similar variance as in Figure 7a,b.

Comparison of the panels in Figure 7 indicates that time averaging and source extent produce similar forms for the PDF of G. This conclusion verifies the notion that, from a statistical point of view, TB-averaging and source extension produce like effects in scintillation fluctuations. The figure also supports the notion that one may use the approximate χ^2 PDF to make calculations rather than solving the Fredholm equation for every case. This is useful because in cases where time and frequency averaging as well as source extent are important, the Fredholm solution may not be obtainable.

4.8. PDF of Visibility Fluctuations

The PDF for G derived in the previous section excludes contributions from source fluctuations such as those that arise from the amplitude modulated noise model. Here we give a nearly exact treatment that takes into account all fluctuations. For simplicity, we assume that observation baselines do not resolve either the source or the seeing disk from the scattering. In this case, we write the average visibility across baseline $\mathbf{b}_{ij}$ between two sites i and j as

$$\overline{\Gamma} \approx G\langle \mathrm{I} \rangle + \langle \mathcal{N}_i \rangle \delta_{ij} + X + C, \tag{23}$$

where $\langle I \rangle$ is the mean source intensity, δ_{ij} is the Kronecker delta, $\langle \mathcal{N} \rangle$ is the mean of $\mathcal{N}_i \equiv |n_i|^2$ (the background noise intensity), X is a real Gaussian RV with zero mean, and C is a complex Gaussian RV with zero mean. Source fluctuations are described by X which includes noise fluctuations associated with $m(\mathbf{r_s}, t)$ and amplitude fluctuations associated with $a(\mathbf{r_s}, t)$ in the amplitude modulated noise model. C includes additive radiometer noise combined with source noise fluctuations, but is uninfluenced by source amplitude fluctuations. Expressions for σ_X^2 and σ_C^2 are given in Appendix C.2.

The PDF for the visibility magnitude is calculated by successively integrating over the PDFs for the different, independent terms in Eq. 23, as done in Appendix C. The PDF for the scaled visibility magnitude, $\gamma = |\overline{\Gamma}|/\sigma_C$, is

$$f_\gamma(\gamma) \;=\; \int dG\, f_G(G) \int dX\, f_X(X) \left[\gamma e^{-\frac{1}{2}(\gamma^2 + G^2 i^2)} I_0(\gamma i) \right]_{i=(\langle \mathrm{I} \rangle + X/G)/\sigma_C} \tag{24}$$

where I_0 is the modified Bessel function. The integrand factor in square brackets is the Rice-Nakagami PDF of a signal phasor added to complex noise (e.g. Thompson, Moran & Swenson 1991, p. 260).

To demonstrate the importance of various terms and factors, we first show, in Figure 8, the visibility PDF when we vary the bandwidth, taking into account that N_{ISS} varies as we do so. There is a tradeoff in discerning the underlying shape of the DISS gain PDF (which encourages use of narrow bandwidths) and maximizing S/N, which favors larger bandwidths: as we decrease the bandwidth there is less averaging of the scintillations but contributions from noise (the X and C terms) increase, thus widening the PDF.

We compare the X and C terms in Eq. 23 with the $G\langle \mathrm{I} \rangle$ term, which dominates when the source is strong. First, we calculate the PDF for $|\overline{\Gamma}|$ with various terms excluded. Figure 9 shows the visibility PDF when there are no DISS and no intrinsic fluctuations, just additive noise. Figure 10 shows the visibility PDF with the intrinsic fluctuations turned on for a fairly high S/N observation, but still with no DISS variations. These curves indicate that source fluctuations can contribute significantly to the shape of the PDF. Figure 11 shows the PDF for different source intensities (top panel) along with (bottom panel) the difference between the true PDF and the PDF where pulsar fluctuations are ignored. The difference vanishes when the source intensity is zero and $\sim 1\%$ for finite source intensities. The error is largest near the peak of the PDF.

Figure 12 shows the PDF when DISS is included with varying numbers of degrees of freedom, $2N_{\rm ISS}$, but with constant bandwidth. This case would apply to observations of sources with different intrinsic sizes or to a point source observed with varying amounts of time averaging. As $N_{\rm ISS} \rightarrow \infty$, the PDF tends toward a Gaussian form. The results indicate that the net PDF for $|\overline{\Gamma}|$ is extremely sensitive to the number of degrees of freedom in the DISS. Also, it is evident that a pure point source can have statistics that mimic those given by an extended source if there is sufficient TB averaging.

Comparison of Figures 12 and 8 indicates that some of the changes in PDF shape evident in Figure 12 that might be due to, say, effects of source size, are indeed masked by any changes in resolution bandwidth in the signal processing.

4.8.1. When is Pulsar Noise Important?

In §C.2 we give expressions for different terms in the visibility variance, including those involving pulsar fluctuations and one involving radiometer noise. All fluctuations diminish, of course, with increased averaging time. However, the relative sizes of the fluctuating terms are independent of the averaging time. In studies of the shape of the visibility or intensity PDF, pulsar fluctuations will be comparable to radiometer noise fluctuations when the pulsar signal strength satisfies

$$G\langle \mathrm{I} \rangle \gtrsim \left(\frac{\langle \mathrm{N}_i \rangle \langle \mathrm{N}_j \rangle}{B\, W_I} \right)^{1/2}, \tag{25}$$

where $\langle \mathrm{I} \rangle$ is the source flux density and W_I is its characteristic time scale (either intrinsic or imposed by some sampling scheme); B is the bandwidth. For a pulsar, W_I would be the sample window in pulse phase and $\langle \mathrm{I} \rangle$ the flux density in that window.

4.9. Cross-Correlation Functions

As described in Appendix B.7, when the intensity is measured for two sources and cross correlated, the total cross modulation index includes only an ISS term because noise and source fluctuations do not correlate. Defining the cross-correlation of the average intensities as in Eq. B27 and defining the cross modulation index as

$$m^2_{\rm cross}(\mathbf{b}, \overline{\tau}) = \frac{C_{\overline{\mathrm{I}},12}(\mathbf{b}, \overline{\tau}) - I_1 I_2}{I_1 I_2}, \tag{26}$$

we find that $m^2_{\rm cross}$ is identically equal to $m^2_{\rm ISS}$ of Eq. 15.

The cross modulation index can be used in two ways to detect source structure or spatial offsets between two sources. First, if its maximum is smaller than unity, quenching of DISS by

source structure is signified. Also, if the cross-modulation maximizes at a time lag $\overline{\tau} \neq 0$ for zero baseline ($\mathbf{b} = 0$), that signifies a significant offset between sources. We show these cases in the Appendix B and will apply this method to pulsar observations in a later paper.

5. Inferring Source Size from Intensity & Visibility Statistics

Given measurements of the visibility of intensity that have time and frequency resolutions that resolve DISS, it is possible to place constraints on source size by comparing visibility fluctuations with those expected from the time and frequency resolutions and as a function of source structure. Here we outline general Bayesian procedures that first analyze visibility/intensity data and then are restricted to a simpler analysis of just the modulation index.

5.1. Likelihood Analysis of Visibility & Intensity Fluctuations

Given a set of visibility (or intensity) measurements

$$\left\{\overline{\Gamma}_i(\mathbf{b}_i), i = 1, N\right\} \tag{27}$$

we can normalize them by the rms off-source noise, σ_C, and use the PDF of $\gamma \equiv \overline{\Gamma}/\sigma_C$ (c.f. Eq. 24) to calculate a likelihood function

$$\mathcal{L} = \prod_i f_\gamma(\gamma_i). \tag{28}$$

The likelihood function depends on numerous parameters that could be estimated by maximizing $\mathcal{L}$. These include parameters that describe the source, $\mathbf{\Theta}_S$, such as source structure and flux density; those that describe wave propagation through the ISM, $\mathbf{\Theta_{ISM}}$, including distances, type of medium (e.g. Kolmogorov), and scintillation parameters ($\Delta\nu_{\rm d}, \Delta t_{\rm d}$); and those that characterize the receiver and telescope system, $\mathbf{\Theta}_{\rm R}$, including the telescope gain and system temperature. Many of these parameters will be known from auxiliary observations.

Denoting all parameters collectively as $\mathbf{\Theta} = (\mathbf{\Theta}_{\rm S}, \mathbf{\Theta}_{\rm ISM}, \mathbf{\Theta}_{\rm R})$, we identify the data probability $P(\mathcal{D}|\mathbf{\Theta})$ as the likelihood function and we calculate, in standard Bayesian fashion (e.g. Gregory & Loredo 1992), the posterior PDF for the parameters as

$$P(\mathbf{\Theta}|\mathcal{D}) \quad = \quad \frac{P(\mathbf{\Theta})P(\mathcal{D}|\mathbf{\Theta})}{\int d\mathbf{\Theta}\, P(\mathbf{\Theta})P(\mathcal{D}|\mathbf{\Theta})} = \frac{\mathcal{L}}{\int d\mathbf{\Theta}\, \mathcal{L}}, \tag{29}$$

where $P(\mathbf{\Theta})$ is the prior PDF for the parameters and the denominator normalizes the PDF. The second equality follows if we assume that the parameters have a flat prior PDF. In the case where, *a priori*, we know many of the parameters, we adopt delta function priors and marginalize them by integrating over those parameters. For example, if we wish to derive the PDF of only source parameters, we would integrate over $d\mathbf{\Theta}_{\rm ISM}\, d\mathbf{\Theta}_{\rm R}$ to obtain $P(\mathbf{\Theta}_{\rm S}|\mathcal{D})$.

To apply this approach we need to solve the multidimensional Fredholm problem that includes source extent and time-bandwidth averaging if we want to use the exact PDF for scintillation gain. Alternatively, we could use the approximate PDF based on the χ^2 PDF (Eq. 20) by calculating the effective number of degrees of freedom associated with source extent and TB averaging. Another, simpler, approach is to analyze only the second moment of the visibility/intensity fluctuations, as we now consider.

5.2. Inferring Source Size from Modulation Indices

The squared modulation index $m_{\rm ISS}^2$ can be calculated through direct estimation of moments or by fitting a PDF shape to a histogram of visibilities (or average intensities). Such estimates of $\hat{m}_{\rm ISS}^2$ are typically made from data that span a large number of scintles, $N_{\rm ISS,TOTAL} \gg 1$. This number is approximately

$$N_{\rm ISS,TOTAL} \approx \left(1 + \zeta \frac{T_{\rm tot}}{\Delta t_{\rm d}}\right)\left(1 + \zeta \frac{B_{\rm tot}}{\Delta \nu_{\rm d}}\right), \tag{30}$$

where the total observing time and bandwidth may be written as $T_{\rm tot} = N_T T$ and $B_{\rm tot} = N_\nu B$, using T and B as the basic resolutions in time and frequency defined previously. The characteristic time and frequency scales for DISS are $\Delta t_{\rm d}$ and $\Delta \nu_{\rm d}$, respectively. The factor $\zeta \approx 0.2 - 0.3$ takes into account that scintles are not packed tightly in the $\nu - t$ plane. In Cordes (1986), I conservatively used $\zeta = 0.1$ whereas a more accurate calculation yields the values presented here.

The fractional estimation error on $\hat{m}_{\rm ISS}^2$ due to the finite number of scintles is $\sigma_{m^2} \approx 2 m_{\rm ISS}^2 N_{\rm ISS,TOTAL}^{-1/2}$. Invoking the Central Limit Theorem for $N_{\rm ISS,TOTAL}$, we expect $\hat{m}_{\rm ISS}^2$ to have PDF, $N(\hat{m}_{\rm ISS}^2, \sigma_{m^2})$.

We write the likelihood function in terms of the PDF for $\hat{m}_{\rm ISS}^2$ estimated from data and using the model for $m_{\rm ISS}^2$ (as given by Eq. 15):

$$\mathcal{L} = \left(2\pi {\sigma_\Gamma}^2\right)^{-1/2} \exp\left\{-\frac{1}{2\sigma_{m^2}}\left[m_{\rm ISS}^2(\mathbf{\Theta}_{\rm S}) - \hat{m}_{\rm ISS}^2\right]^2\right\}, \tag{31}$$

where $\mathbf{\Theta}_{\rm S}$ is a vector of parameters that represents the source structure. Bayes' theorem can then be applied according to Eq. 29 to derive the posterior PDF for $\mathbf{\Theta}_{\rm S}$. For the Gaussian brightness distribution of Eq 18, the posterior PDF is simply a one-dimensional PDF $f_{\sigma_r}(\sigma_r)$ for the sole source parameter σ_r.

Uncertainties in the application of this inference scheme include the systematic errors associated with not knowing the true form of the structure function for the medium and also the statistical errors in the measured modulation index, $\hat{m}_{\rm ISS}^2$ and in the DISS parameters $\Delta \nu_{\rm d}$ and $\Delta t_{\rm d}$. We address these uncertainties in Paper II.

6. Summary and Conclusions

We have derived a general methodology for analyzing diffractive interstellar scintillation fluctuations that is applicable to single aperture and interferometric observations. In this paper, we considered only the strong scattering regime where the scattered wavefield has Gaussian statistics. The method explicitly takes into account time-bandwidth averaging that is often used in the statistical analysis of such observations. Such averaging modifies the statistics in a way that is identical to the effects of extended source structure. We show that time-bandwidth averaging and extended source structure both increase the number of degrees of freedom in the scintillations from the minimum value of two that describes the fully modulated, Gaussian wavefield of the scintillations.

Our methodology can be applied to any radio source in the strong scattering regime, including compact active galactic nuclei and gamma-ray burst afterglows. In another paper, we will address sources of these types and we will also consider scintillations in the weak and transition scattering regimes.

In Paper II we apply our results to the recent VLBI observations of the Vela pulsar by Gwinn *et al.* (1997) and find that the scintillation statistics may be accounted for fully by time-bandwidth averaging. Any contribution from extended source structure is less than an upper limit of about 400 km at the 95% confidence interval. This upper limit on the transverse extent is substantially larger than the size expected from conventional models that place radio emission well within the light cylinder of the pulsar and close to the surface of the neutron star.

I thank Z. Arzoumanian, S. Chatterjee, C. R. Gwinn, H. Lambert, M. McLaughlin, and B. J. Rickett for useful discussions and H. Lambert and B. J. Rickett for making available their numerically-derived autocovariance functions for Kolmogorov media. This research was supported by NSF grant 9819931 to Cornell University and by NAIC, which is managed by Cornell University under a cooperative agreement with the NSF.

APPENDICES

A. Scintillating Amplitude Modulated Noise Model

Here we derive a general statistical model that incorporates incoherent summing in the source and wave propagation throughout the interstellar medium.

The narrowband (scalar) electric field incident on an aperture and selected by a feed antenna and by a bandpass receiver may be written in the form

$$E_\Delta(t) = Re\left\{\varepsilon(t)\exp(-i\omega_0 t)\right\}, \tag{A1}$$

where ω_0 is the center frequency and the complex, baseband wavefield is ε (e.g. Thomas 1969). The baseband field is often explicitly extracted through quadrature mixing schemes in heterodyned radio receivers (e.g. Thompson, Moran & Swenson 1991, p. 150).

Early work on pulsars modeled $\varepsilon(t)$ as amplitude modulated noise (AMN) with additive background and receiver noise:

$$\varepsilon(t) = a(t)m(t) + n(t), \tag{A2}$$

where m and n are complex, Gaussian wavefields that describe intrinsic source noise and additive noise, respectively. The factor $a(t)$ is a real modulation function that describes source variations on time scales much longer than the reciprocal center frequency or reciprocal bandwidth; otherwise the statistics of $a(t)$ are arbitrary. The additive noise has a modulation index $m_N = [\langle|m|^4\rangle/\langle|m|^2\rangle^2 - 1]^{1/2} = 1$.

The AMN model was first presented by Rickett (1975), who attributed complex, Gaussian statistics to $m(t)$. For this case the modulation index is also unity, $m_M = 1$. Cordes (1976b) considered Poissonian shot-noise statistics for $m(t)$ based on physical models for pulsar emission; for Poissonian noise, $m_M \geq 1$.

Empirical tests on pulsars (Cordes 1976a; Hankins & Boriakoff 1978; Cordes & Hankins 1979; Bartel & Hankins 1982) show consistency of $m(t)$ with Gaussian statistics on time scales as short as $\sim 1\ \mu s$. Tests in the time domain resort to investigation of the relative amplitudes of various terms in the autocorrelation function of the intensity (Rickett 1975; Cordes 1976a; Bartel & Hankins 1982). Tests in the frequency domain, with the same conclusion, use the autocorrelation function of the spectrum (Cordes & Hankins 1979). The model predicts that there is frequency structure in the spectrum of a single pulse with characteristic bandwidth equal to the reciprocal of the time duration of $a(t)$. This frequency structure averages out as multiple pulses are summed.

Tests on OH and H_2O masers (Evans *et al.* 1972; Moran 1981) show that maser emission also conforms to the AMN picture. It is expected that *any* radio source can be described by AMN because large numbers of particles contribute to the observed signals and most, if not all, natural

sources involve incoherent superposition of radiation from incoherent or coherent emissions from individual radiators. Thus AMN should apply to gamma-ray burst sources and the most compact AGNs that show intra-day variability.

A.1. Amplitude Modulated Noise for Extended Sources

We model extended sources as follows. First, the baseband field produced by a point source at location $(\mathbf{r_s}, z = 0)$ is

$$\varepsilon_s(\mathbf{r_s}, t) = a(\mathbf{r_s}, t) m(\mathbf{r_s}, t), \tag{A3}$$

where $a(\mathbf{r_s}, t)$ is the (real) amplitude modulation and $m(\mathbf{r_s}, t)$ is complex Gaussian noise (Rickett 1975). Here and everywhere, vectors are two dimensional and perpendicular to the line of sight. The quantity ε_s is the field emitted per unit area at the source, uninfluenced by propagation (either through free space or a turbulent medium), except that we include the dependence on distance from the source on its mean amplitude, for simplicity. For a steady source, $a(\mathbf{r_s}, t)$, is constant in time. For pulsars, it describes the periodic envelope of pulses that modulates the underlying noise process, $m(\mathbf{r_s}, t)$. The corresponding mean intensity is, using $A \equiv a^2$,

$$I_s(\mathbf{r_s}, t) = \langle |\varepsilon_s(\mathbf{r_s}, t)|^2 \rangle = \langle A(\mathbf{r_s}, t) \rangle. \tag{A4}$$

In most of this paper we assume stationary statistics, so $I_s(\mathbf{r_s}, t) \to I_s(\mathbf{r_s})$.

The total measured field is the integral over source components

$$\varepsilon(\mathbf{r}, t) = \int d\mathbf{r_s}\, \varepsilon_s(\mathbf{r_s}, t) g(\mathbf{r}, t, \nu, \mathbf{r_s}), \tag{A5}$$

where we include a multiplicative propagation factor, $g(\mathbf{r}, t, \nu, \mathbf{r_s})$, defined in the next section.

The noise, with stationary statistics, has a correlation function

$$\Gamma_{2m}(\mathbf{r_{s1}}, \mathbf{r_{s2}}, t_1, t_2) = \langle m(\mathbf{r_{s1}}, t_1) m^*(\mathbf{r_{s2}}, t_2) \rangle = \delta(\mathbf{r_{s1}} - \mathbf{r_{s2}}) \Delta(t_2 - t_1), \tag{A6}$$

where the asterisk denotes conjugation and $\Delta(\tau)$ is an Hermitian function having unit amplitude, $\Delta(0) = 1$, and width approximately equal to the inverse of the receiver bandwidth. Angular brackets denote an ensemble average, except where noted. The noise fourth moment is the standard dual sum of products for a complex Gaussian process,

$$\begin{aligned} \Gamma_{4m}(\mathbf{r_{s1}}, \mathbf{r_{s2}}, \mathbf{r_{s3}}, \mathbf{r_{s4}}, t_1, t_2, t_3, t_4) &= \langle m(\mathbf{r_{s1}}, t_1) m^*(\mathbf{r_{s2}}, t_2) m(\mathbf{r_{s3}}, t_3) m^*(\mathbf{r_{s4}}, t_4) \rangle \\ &= \Gamma_{2m}(\mathbf{r_{s1}}, \mathbf{r_{s2}}, t_1, t_2) \Gamma_{2m}(\mathbf{r_{s3}}, \mathbf{r_{s4}}, t_3, t_4) \\ &+ \Gamma_{2m}(\mathbf{r_{s1}}, \mathbf{r_{s4}}, t_1, t_4) \Gamma^*_{2m}(\mathbf{r_{s2}}, \mathbf{r_{s3}}, t_2, t_3). \end{aligned} \tag{A7}$$

A.2. Propagation Through a Thin Diffracting Screen

Consider the following geometry: a point source at $(\mathbf{r_s}, 0)$, a thin screen at $(\mathbf{r}', D_s)$ and an observer at $(\mathbf{r}, d = D_s + D)$. The screen changes only the phase of incident waves. Under the narrowband approximation ($\Delta\nu \ll \nu$) (so that all phase factors may be considered constant over the band) the propagated baseband field for a point source at $\mathbf{r_s}$ is (e.g. Goodman 1985)

$$\varepsilon(\mathbf{r}, t, \mathbf{r_s}) = (i\lambda\overline{D})^{-1} \int d\mathbf{r}'\, e^{i\phi(\mathbf{r}', t - c^{-1}\mathcal{D}_{23})} e^{ik\mathcal{D}_{13}} \varepsilon_s(\mathbf{r_s}, t - c^{-1}\mathcal{D}_{13}), \tag{A8}$$

where $\overline{D} \equiv ({D_s}^{-1} + D^{-1})^{-1}$ and the integral is normalized so that a screen with zero phase yields simply a delayed version of the emitted field, $\varepsilon_s(\mathbf{r_s}, t - c^{-1}d)$. Under the paraxial approximation (transverse scales much smaller than line-of-sight distances),

$$\begin{aligned} \mathcal{D}_{13} &= \mathcal{D}_{12} + \mathcal{D}_{23} \\ \mathcal{D}_{12} &\approx D_s + \frac{|\mathbf{r}' - \mathbf{r_s}|^2}{2D_s} \\ \mathcal{D}_{23} &\approx D + \frac{|\mathbf{r} - \mathbf{r}'|^2}{2D}. \end{aligned}$$

We assume further that variations in propagation times, $c^{-1}\mathcal{D}_{13}$ and $c^{-1}\mathcal{D}_{23}$ (as a function of relevant source locations $\mathbf{r_s}$ and screen exit points $\mathbf{r}'$) are negligible compared to the characteristic variation time scales for $\phi(\mathbf{r}', t)$ and $\varepsilon(\mathbf{r_s}, t)$. $c^{-1}\Delta\nu(\mathcal{D}_{13} - d) \ll 1$. Typically, ε_s varies on time scales of order the reciprocal bandwidth (e.g. 100 μs or less) while g varies, due to the changing geometry, on time scales of seconds to hours or more, for the situations we wish to consider. Therefore, for ε_s to be factored out of the integral, we require $c^{-1}\Delta\nu(\mathcal{D}_{13} - d) \ll 1$. This simply means that any time smearing from differential arrival times must be less than the time resolution of the signal. Though we assume in the remainder that the inequality is satisfied, we point out that there are many instances where it is not, corresponding to the well known 'pulse broadening' effect (e.g. Rickett 1990). As a rule of thumb, when pulse broadening is important, scintillations are difficult to resolve in time and frequency. And when scintillations are important, the pulse broadening can be too small to be important, as we assume here.

We can now write the propagated field for a single point source as

$$\varepsilon(\mathbf{r}, t, \mathbf{r_s}) = \varepsilon_s(\mathbf{r_s}, t - d/c) g(\mathbf{r}, t - D/c, \nu, \mathbf{r_s}), \tag{A9}$$

where g is the propagator,

$$g(\mathbf{r}, t, \nu, \mathbf{r_s}) = (i\lambda\overline{D})^{-1} \int d\mathbf{r}'\, \exp\left\{ i \left[\frac{k}{2} \left({D_s}^{-1} |\mathbf{r}' - \mathbf{r_s}|^2 + D^{-1} |\mathbf{r} - \mathbf{r}'|^2 \right) + \phi(\mathbf{r}', t) \right] \right\}, \tag{A10}$$

and we use $k = 2\pi c^{-1}\nu$. The normalization of g yields it to be simply a unit modulus phase factor when the screen phase is zero and also it yields $\langle |g|^2 \rangle = 1$ when the screen phase has Gaussian statistics. In the following we will ignore the delays d/c and D/c in Eq. A9 in our notation.

The time dependence of $g(\mathbf{r}, t, \nu, \mathbf{r_s})$ arises from motions of source, observer and medium, which influence all terms in the exponent in the integrand. Absent any random phase screen (i.e. $\phi = 0$), g is simply a complex phase factor that describes free-space propagation,

$$g(\mathbf{r}, t, \nu, \mathbf{r_s}) = e^{ik|\mathbf{r_s}-\mathbf{r}|^2/2d}. \tag{A11}$$

A.3. Propagator Second Moment for a Thin Screen

The propagator's second moment across a baseline $\mathbf{b}$, at two times separated by τ for two point sources at $\mathbf{r_{s1,2}}$ and at two frequencies separated by $\delta\nu$ is

$$\begin{aligned}
\Gamma_g(\mathbf{b}, \tau, \delta\nu, \delta\mathbf{r_s}) &= \langle g(\mathbf{r}, t, \nu, \mathbf{r_s}) g^*(\mathbf{r}+\mathbf{b}, t+\tau, \nu+\delta\nu, \mathbf{r_s}+\delta\mathbf{r_s})\rangle \\
&= e^{-i\psi}\gamma_{\rm g}(\mathbf{b}, \tau, \delta\nu, \delta\mathbf{r_s}) && \text{(A12)} \\
\psi &= kd^{-1}\{(\mathbf{r_s}-\mathbf{r})\cdot\Delta\mathbf{R} + \frac{1}{2}|\Delta\mathbf{R}|^2\} && \text{(A13)} \\
\Delta\mathbf{R} &= [\delta\mathbf{r_s} - \mathbf{b} + (\mathbf{V_p} - \mathbf{V_{obs}})\tau]. && \text{(A14)}
\end{aligned}$$

There is no term $\propto \Delta\nu$ in ψ because it is negligible according to the narrowband assumption made earlier, i.e. that $c^{-1}\Delta\nu(\mathcal{D}_{13} - d) \ll 1$.

The real, second moment $\gamma_{\rm g}$ for zero frequency lag is

$$\gamma_{\rm g}(\mathbf{b}, \tau, \delta\nu = 0, \delta\mathbf{r_s}) = e^{-\frac{1}{2}D_\phi(\mathbf{b}, \tau, \delta\mathbf{r_s})} \tag{A15}$$

where the phase structure function D_ϕ and its arguments are given by

$$\begin{aligned}
D_\phi(\mathbf{b}, \tau, \delta\mathbf{r_s}) &\equiv \left\langle [\phi(\mathbf{r}, t) - \phi(\mathbf{r}+\mathbf{b}_{\rm eff}, t)]^2 \right\rangle = \left(\frac{b_{\rm eff}}{b_e}\right)^\alpha && \text{(A16)} \\
\mathbf{b}_{\rm eff} &= (D_s/d)\mathbf{b} + \mathbf{V}_{\rm eff}\tau + (D/d)\delta\mathbf{r_s} && \text{(A17)} \\
\mathbf{V}_{\rm eff} &= (D_s/d)\mathbf{V_{obs}} + (1 - D_s/d)\mathbf{V_p} - \mathbf{V_m} && \text{(A18)}
\end{aligned}$$

The scaling exponent for the structure function, D_ϕ, is α, which takes on a value $\alpha = 5/3$ for a Kolmogorov spectrum in some instances. The e^{-1} scale of $|\gamma_{\rm g}|^2$ is b_e, $\mathbf{V_p}$ is the pulsar velocity, $\mathbf{V_{obs}}$ is the observer's velocity and $\mathbf{V_m}$ is the velocity of the scattering material in the ISM. The normalized autocovariance function for $G = |g|^2$, which we call the intensity "gain," is (in the strong scattering, or Rayleigh, regime)

$$\gamma_{\rm G}(\mathbf{b}, \tau, \delta\nu, \delta\mathbf{r_s}) \equiv \langle G(\mathbf{r}, t, \nu, \mathbf{r_{s1}})\, G(\mathbf{r}+\mathbf{b}, t+\tau, \nu+\delta\nu, \mathbf{r_{s2}}) - 1 = |\gamma_{\rm g}(\mathbf{b}, \tau, \delta\nu, \delta\mathbf{r_s})|^2, \tag{A19}$$

and the mean intensity is

$$I(\mathbf{r}, t) = \int d\mathbf{r_s}\, I_s(\mathbf{r_s}, t) = \int d\mathbf{r_s}\, \langle A(\mathbf{r_s}, t)\rangle. \tag{A20}$$

Note that $\langle G \rangle = 1$. We emphasize that the form for $\gamma_{\rm g}$ in the second equalities of Eq. A12 and Eq. A19 relies on the assumption that the scattered wavefield is sufficiently randomized that Gaussian statistics apply.

For nonzero frequency lags, $\gamma_{\rm g}$ generally must be obtained through appropriate numerical integration (e.g. Lambert & Rickett 1999; Lee & Jokipii 1975). For the special case of a square-law structure function, a closed form expression is available for a thin screen (Chashei & Shishov 1976; Cordes *et al.* 1986; Gupta *et al.* 1994).

A.4. Extension to An Arbitrarily Thick Medium

The results presented so far were derived explicitly for a thin screen. For a medium in which scattering occurs with variable strength all along the line of sight, the results may be extrapolated quite simply and generally. Assuming that the net measured field is still Gaussian, it is a matter of simple geometry to work out the form of the equivalent phase structure function. Following Lotova & Chashei (1981) and Cordes & Rickett (1998) we use the same results as in Eq. A12-A26 but make the replacements,

$$D_\phi(\mathbf{b}, \tau, \delta\mathbf{r_s}) = (\lambda r_e)^2 f_\alpha \int_0^d ds\, C_n^2(s) |\mathbf{b}_{\rm eff}(s)|^\alpha \tag{A21}$$

$$\mathbf{b}_{\rm eff}(s) = (s/d)\mathbf{b} + \mathbf{V}_{\rm eff}(s)\tau + (1 - s/d)\delta\mathbf{r_s} \tag{A22}$$

$$\mathbf{V}_{\rm eff}(s) = (s/d)\mathbf{V}_{\rm obs} + (1 - s/d)\mathbf{V}_{\rm p} - \mathbf{V}_{\rm m}(s), \tag{A23}$$

where

$$f_\alpha = \frac{8\pi^2}{\alpha 2^\alpha} \frac{\Gamma(1 - \alpha/2)}{\Gamma(1 + \alpha/2)}. \tag{A24}$$

and C_n^2 is the coefficient in the wavenumber spectrum for electron density variations (Cordes & Lazio 1991; Armstrong, Rickett & Spangler 1995). For the case $C_n^2(s) \propto \delta(s - D_s)$, we retrieve the thin-screen results of the previous section.

A.5. Visibility Function

The ensemble mean visibility function is the product of the true source visibility and the propagator's second moment (ignoring a phase factor)

$$\langle \Gamma_\varepsilon(\mathbf{b}, t, \tau_i) \rangle = \langle \varepsilon(\mathbf{r}, t) \varepsilon^*(\mathbf{r} + \mathbf{b}, t + \tau_i) = \Delta(\tau_i) \gamma_{\rm g}(\mathbf{b}, 0, 0, 0) \Gamma_s(\mathbf{b}, t), \tag{A25}$$

where we have designated the interferometer lag as τ_i. This must match any geometrical time delays to within the reciprocal of the receiver bandwidth. The source visibility is the usual Fourier transform of the brightness distribution,

$$\Gamma_s(\mathbf{b}, t) = \int d\mathbf{r_s}\, e^{+ikd^{-1}\mathbf{r_s}\cdot\mathbf{b}} I_s(\mathbf{r_s}, t). \tag{A26}$$

The time lag τ_i in Eq. A25 is zero to within a very small time (of order the reciprocal bandwidth; see Thompson, Moran & Swenson 1991). By contrast, the time lag in Eq. A12 extends over very long times, seconds to hours, that characterize DISS fluctuations.

B. Intensity & Visibility Fluctuations

Here we consider variations in the time-averaged intensity and visibility for the model of Appendix A. We derive the modulation fractions of these quantities taking into account scintillations and intrinsic and additive noise. Our expressions will include any averaging of the scintillation modulation over frequency as well as time.

We define the general fourth moment for the narrowband field ε (*sans* additive noise)

$$R_{4\varepsilon}(\mathbf{b}, t_1, t_2, t_3, t_4) \quad = \quad \langle \varepsilon(\mathbf{r}, t_1)\varepsilon^*(\mathbf{r}, t_2)\varepsilon(\mathbf{r}+\mathbf{b}, t_3)\varepsilon^*(\mathbf{r}+\mathbf{b}, t_4)\rangle, \tag{B1}$$

where $\varepsilon(\mathbf{r}, t)$ is given by Eq. A5. Expanding out, $R_{4\varepsilon}$ involves fourth-order moments of $a(\mathbf{r_s}, t)$ and $m(\mathbf{r_s}, t)$ from the AMN model of Appendix A and of the propagator $g(\mathbf{r}, t, \nu, \mathbf{r_s})$. We use the fact that a, m, and g are statistically independent. Also, m and g are complex gaussian processes so their fourth moments are dual sums of products of their second moments, as in Eq. A7.

The fourth moment of of $a(\mathbf{r_s}, t)$ ends up as the second moment of its square, $A \equiv a^2$, which we assume has the form

$$\langle A(\mathbf{r_{s1}}, t_1)A(\mathbf{r_{s2}}, t_2)\rangle = \langle A(\mathbf{r_{s1}}, t_1)\rangle\langle A(\mathbf{r_{s2}}, t_2)\rangle[1 + m_A^2\rho_A(\mathbf{r_{s2}} - \mathbf{r_{s1}}, t_2 - t_1)]. \tag{B2}$$

This form assumes stationary statistics for A with a correlation function ρ_A and modulation index m_A. As we show in paper II, assuming stationary statistics is not restrictive, even for pulsars which are highly nonstationary across pulse phase but appear to have stationary statistics when a fixed pulse phase is considered. For other radio sources with intrinsic variations much longer than those of pulsars, we may consider $\langle A(\mathbf{r_s}, t)\rangle$ to be constant in time, with $m_A = 0$, at least over a typical observation time of minutes.

Our treatment also includes any variations of the scintillation propagator, g, across the bandwidth of the narrowband signal, $\varepsilon(\mathbf{r}, t)$. By partitioning ε into subbands in which the propagator is piecewise constant and between which the emitted signal ε_s is statistically independent, we easily can incorporate finite bandpass effects while being consistent with our earlier assumption about the narrowband signal.[3]

B.1. Autocorrelation Functions of Time Average Quantities

The time-averaged intensity,

$$\overline{\mathrm{I}}(\mathbf{r}, t) = T^{-1}\int_{t-T/2}^{t+T/2} dt'\, I(\mathbf{r}, t'), \tag{B3}$$

[3]The net effect is that intensities from the subbands add while the intensity autocorrelation function discussed later involves an average over frequency lag.

has autocorrelation function

$$R_{\overline{\mathrm{I}}}(\mathbf{b},\tau) \equiv \langle \overline{\mathrm{I}}(\mathbf{r},t)\overline{\mathrm{I}}(\mathbf{r}+\mathbf{b},t+\tau)\rangle = T^{-2}\int\int_{t-T/2}^{t+T/2} dt_a\, dt_b\, \mathrm{R_I}(\mathbf{b}, t_b - t_a + \tau) \quad \text{(B4)}$$

$$= T^{-1}\int_{-T}^{+T} d\tau' \left(1 - \frac{|\tau'|}{T}\right) \mathrm{R_I}(\mathbf{b},\tau'+\tau). \quad \text{(B5)}$$

The integrand is given by

$$\mathrm{R_I}(\mathbf{b},\tau) = R_{4\varepsilon}(\mathbf{b}, t_1, t_1, t_1+\tau, t_1+\tau). \quad \text{(B6)}$$

Similarly, we consider the visibility,

$$\Gamma_\varepsilon(\mathbf{b},t,\tau_i) = \varepsilon(\mathbf{r},t)\varepsilon^*(\mathbf{r}+\mathbf{b},t+\tau_i) \quad \text{(B7)}$$

and its time average,

$$\overline{\Gamma}(\mathbf{b},t,\tau_i) = T^{-1}\int_{t-T/2}^{t+T/2} dt'\, \overline{\Gamma}(\mathbf{b},t',\tau_i). \quad \text{(B8)}$$

The autocorrelation, analogous to Eq. B5, is

$$R_{\overline{\Gamma}}(\mathbf{b},\overline{\tau};\tau_i) = T^{-1}\int_{-T}^{+T} d\tau' \left(1 - \frac{|\tau'|}{T}\right) R_{\overline{\Gamma}}(\mathbf{b},\tau'+\overline{\tau};\tau_i), \quad \text{(B9)}$$

and involves the integrand

$$R_{\overline{\Gamma}}(\mathbf{b},\overline{\tau};\tau) = R_{4\varepsilon}(\mathbf{b}, t_1, t_1+\overline{\tau}, t_1+\overline{\tau}+\tau, t_1+\tau). \quad \text{(B10)}$$

Note that we distinguish here between the lag associated with the definition of the visibility, τ_i, and the lag $\overline{\tau}$ with which we consider the autocorrelation of the visibility.

B.2. Modulation Indices

We are most interested in the normalized variances of the time-average intensity and visibility. These are defined in terms of the autocorrelation functions as

$$m^2_{\overline{\mathrm{I}}}(\mathbf{b},\tau) \equiv \frac{R_{\overline{\mathrm{I}}}(\mathbf{b},\tau) - \langle \mathrm{I}\rangle^2}{\langle \mathrm{I}\rangle^2} \quad \text{(B11)}$$

$$m^2_{\overline{\Gamma}}(\mathbf{b},\tau) \equiv \frac{R_{\overline{\Gamma}}(\mathbf{b},\tau) - |\langle \Gamma_\varepsilon\rangle|^2}{\langle \mathrm{I}\rangle^2}, \quad \text{(B12)}$$

where we normalize by the mean intensity in both cases.

The total modulation index squared for the intensity or visibility is the sum of three main terms:

$$m^2(\mathbf{b},\overline{\tau}) = m^2_{\mathrm{ISS}}(\mathbf{b},\overline{\tau}) + m^2_{\mathrm{PSR}}(\mathbf{b},\overline{\tau}), + m^2_{\mathrm{NOISE}}(\mathbf{b},\overline{\tau}), \quad \text{(B13)}$$

where $m^2_{\rm ISS}$ measures the contribution from scintillations only, $m^2_{\rm PSR}$ measures the contribution from source amplitude fluctuations combined with scintillations, and $m^2_{\rm NOISE}$ measures source noise fluctuations. Later (§B.6) we will also consider the effects of additive radiometer fluctuations. For pulsars, $m^2_{\rm PSR}$ includes pulse shape variations and noise fluctuations. For sources that are steady over an observation span of minutes to hours (or more), $m^2_{\rm PSR} = 0$. The 'noise' term, $m^2_{\rm NOISE}$, depends on source structure and corresponds to the output of an intensity interferometer that is proportional to the square of the visibility function (e.g. Hanbury-Brown 1974, pp. 48-49).

We can write these terms as

$$m^2_{\rm ISS}(\mathbf{b},\overline{\tau}) = \langle {\rm I}\rangle^{-2} \int\int d\mathbf{x}\, d\mathbf{y}\, {\rm I}_{\mathbf{r_s}}(\mathbf{x}){\rm I}_{\mathbf{r_s}}(\mathbf{y}) Q_{\rm ISS}(\mathbf{b},\overline{\tau},\mathbf{y}-\mathbf{x},T,B) \tag{B14}$$

$$m^2_{\rm PSR}(\mathbf{b},\overline{\tau}) = \langle {\rm I}\rangle^{-2} \int\int d\mathbf{x}\, d\mathbf{y}\, {\rm I}_{\mathbf{r_s}}(\mathbf{x}){\rm I}_{\mathbf{r_s}}(\mathbf{y}) Q_{\rm PSR}(\mathbf{b},\overline{\tau},\mathbf{y}-\mathbf{x},T,B) \tag{B15}$$

$$m^2_{\rm NOISE}(\mathbf{b},\overline{\tau}) = \langle {\rm I}\rangle^{-2} \int\int d\mathbf{x}\, d\mathbf{y}\, {\rm I}_{\mathbf{r_s}}(\mathbf{x}){\rm I}_{\mathbf{r_s}}(\mathbf{y}) Q_{\rm NOISE}(\mathbf{b},\overline{\tau},\mathbf{y}-\mathbf{x},T,B) \tag{B16}$$

The 'Q' functions are defined in terms of integrals over time lag, like that in Eq. B5 and over similar frequency-lag integrals, that we denote as

$$\langle X(y)\rangle_{y,Y} \equiv Y^{-1}\int_{-Y}^{+Y} dy\, \left(1-\frac{|y|}{Y}\right) X(y). \tag{B17}$$

B.3. Intensity Fluctuations

For intensity fluctuations, the Q functions are

$$Q_{\rm ISS}(\mathbf{b},\overline{\tau},\delta\mathbf{r_s},T,B) = \left\langle \gamma_{\rm G}(\mathbf{b},\tau'+\overline{\tau},\delta\nu,\delta\mathbf{r_s})\right\rangle_{\tau',T;\ \delta\nu,B}, \tag{B18}$$

$$\begin{aligned} Q_{\rm PSR}(\mathbf{b},\overline{\tau},\delta\mathbf{r_s},T,B) = {} & \\ & m_A^2\left\{\left\langle\rho_A(\delta\mathbf{r_s},\tau'+\overline{\tau})\right\rangle_{\tau',T} + \left\langle\rho_A(\delta\mathbf{r_s},\tau'+\overline{\tau})\gamma_{\rm G}(\mathbf{b},\tau'+\overline{\tau},\delta\nu,\delta\mathbf{r_s})\right\rangle_{\tau',T;\ \delta\nu,B}\right. \\ & \left. + R_\Delta(\overline{\tau},T)e^{-ikd^{-1}\mathbf{b}\cdot\delta\mathbf{r_s}}\rho_A(\delta\mathbf{r_s},0)\left[\gamma_{\rm G}(\mathbf{b},0,0,0)+\left\langle\gamma_{\rm G}(0,0,\delta\nu,\delta\mathbf{r_s})\right\rangle_{\delta\nu,B}\right]\right\}, \end{aligned} \tag{B19}$$

$$Q_{\rm NOISE}(\mathbf{b},\overline{\tau},\delta\mathbf{r_s},T,B) = R_\Delta(\overline{\tau},T)e^{-ikd^{-1}\mathbf{b}\cdot\delta\mathbf{r_s}}\left[\gamma_{\rm G}(\mathbf{b},0,0,0)+\left\langle\gamma_{\rm G}(0,0,\delta\nu,\delta\mathbf{r_s})\right\rangle_{\delta\nu,B}\right]. \tag{B20}$$

We have made use of the lag-integrated noise correlation

$$R_\Delta(\tau,T) \equiv T^{-1}\int_{-T}^{T} d\tau'\, \left(1-\frac{\tau'}{T}\right)|\Delta(\tau')|^2. \tag{B21}$$

Recall that $\Delta(\tau)$ is a function with unit maximum amplitude [$\Delta(0)=1$] and width of order the reciprocal bandwidth, B^{-1}. For integration times $T \gg B^{-1}$, we have

$$R_\Delta(\tau,T) \approx \frac{W_\Delta}{T}U(T-\tau)U(T+\tau), \tag{B22}$$

where $U(x)$ is the unit step function and $W_\Delta \equiv \int d\tau\, |\Delta(\tau)|^2 \approx B^{-1}$ is the characteristic time scale of the noise fluctuations.

Note that for $T \gg W_\Delta$, the terms involving R_Δ in $Q_{\rm PSR}$ and $Q_{\rm NOISE}$ are much smaller than $Q_{\rm ISS}$. Also, for radio sources other than pulsars, $Q_{\rm PSR} \equiv 0$ because $m_A = 0$.

B.4. Intensity Interferometry

We can relate our results to those of Hanbury-Brown and Twiss (e.g. Hanbury Brown 1974), who used the intensity autocorrelation function to determine the magnitude of the source visibility function for optical stars. The term of interest in their work corresponds to our $Q_{\rm NOISE}$, in particular the second term which involves $\langle \gamma_{\rm G}(0,0,\delta\nu,\delta\mathbf{r_s})\rangle_{\delta\nu,B}$. The first term with $\gamma_{\rm G}(\mathbf{b},0,0,0)$ vanishes for baselines much larger than the Fried scale. Also, the apertures used by Hanbury Brown and Twiss were larger than the Fried scale, causing aperture averaging that we have not treated but which is analogous to time-bandwidth averaging. For ground-based optical observations of stars, Hanbury-Brown and Twiss used a bandwidth such that scintillations were constant over the band and the stars they observed were much smaller than the isoplanatic scale. In this case, $\gamma_{\rm G}(0,0,\delta\nu,\delta\mathbf{r_s}) \to 1$ and the effect was maximized. Note also, however, that the amplitude of the effect scales with $R_\Delta(\overline{\tau},T) \approx W_\Delta/T \approx (BT)^{-1}$, which is small for significant time-bandwidth averaging.

B.5. Visibility Fluctuations

For the visibility we have, using $\mathbf{\Delta V} \equiv \mathbf{V}_{\rm p} - \mathbf{V}_{\rm obs}$,

$$Q_{\rm ISS}(\mathbf{b},\overline{\tau},\delta\mathbf{r_s},T,B) = |\Delta(\tau_i)|^2 \left\langle \gamma_{\rm G}(0,\tau'+\overline{\tau},\delta\nu,\delta\mathbf{r_s}) e^{-ikd^{-1}\mathbf{b}\cdot[\delta\mathbf{r_s}+\mathbf{\Delta V}(\tau'+\overline{\tau})]} \right\rangle_{\tau',T;\ \delta\nu,B} \quad \text{(B23)}$$

$$Q_{\rm PSR}(\mathbf{b},\overline{\tau},\delta\mathbf{r_s},T,B) = \quad \text{(B24)}$$

$$\begin{aligned} & m_A^2 \left\{ |\Delta(\tau_i)|^2 e^{-ikd^{-1}\mathbf{b}\cdot\delta\mathbf{r_s}} \langle \rho_A(\delta\mathbf{r_s},\tau'+\tau)\gamma_{\rm G}(\mathbf{b},0,0,0)\rangle_{\tau',T} \right. \\ & + \left\langle \rho_A(\delta\mathbf{r_s},\tau'+\tau)\gamma_{\rm G}(0,\tau'+\overline{\tau},\delta\nu,\delta\mathbf{r_s}) e^{-ikd^{-1}\mathbf{b}\cdot[\mathbf{\Delta V}(\tau'+\overline{\tau})]} \right\rangle_{\tau',T;\ \delta\nu,B} \\ & \left. + R_\Delta(\overline{\tau},T)\rho(\delta\mathbf{r_s},0) \left[1 + \langle \gamma_{\rm G}(\mathbf{b},\tau_i,\delta\nu,\delta\mathbf{r_s})\rangle_{\delta\nu,B} \right] \right\}. \end{aligned}$$

$$Q_{\rm NOISE}(\mathbf{b},\overline{\tau},\delta\mathbf{r_s},T,B) = R_\Delta(\tau,T) \left[1 + \langle \gamma_{\rm G}(\mathbf{b},\tau_i,\delta\nu,\delta\mathbf{r_s})\rangle_{\delta\nu,B} \right]. \quad \text{(B25)}$$

B.6. Effects of Additive Noise

Results given so far for intensity and visibility fluctuations have considered only the signal emitted by the source. Including the additive radiometer noise n as in Eq. A2, we obtain an additional contribution to the total modulation index, that we denote m_{rad}^2: For the time-average

intensity and visibility, the contribution is

$$m^2_{rad}(\mathbf{b}_{ij},\overline{\tau}) = \begin{cases} 2\langle \mathrm{I}\rangle^{-1}\langle \mathrm{N}_i\rangle \delta_{ij} R_\Delta(\overline{\tau},T)\left(1+\frac{1}{2}\langle \mathrm{I}\rangle^{-1}\langle \mathrm{N}_i\rangle\right) & \text{intensity fluctuations} \\ \\ \langle \mathrm{I}\rangle^{-1}\langle \mathrm{N}_i\rangle R_\Delta(\overline{\tau},T)\left(1+\frac{\langle \mathrm{N}_j\rangle}{\langle \mathrm{N}_i\rangle}+\langle \mathrm{I}\rangle^{-1}\langle \mathrm{N}_j\rangle\right) & \text{visibility fluctuations} \end{cases} \tag{B26}$$

We have labelled the baseline with ij indices to represent the ith and jth sites. The Kronecker delta indicates that the contribution for the intensity holds only for single-site measurements for which i and j are equal.

B.7. Cross Correlations of Time-Average Intensities

In some circumstances, we are interested in the cross correlation function of the intensity between two sources that may or may not be scintillating together. Pulsars, for example, have different pulse components that may come from spatially different emission regions and it is possible to record or compute intensities for each component separately and cross-correlate them. We define the cross correlation as

$$C_{\overline{\mathrm{I}},12}(\mathbf{b},\overline{\tau}) \equiv \langle \overline{\mathrm{I}}_1(\mathbf{r},t)\overline{\mathrm{I}}_2(\mathbf{r}+\mathbf{b},t+\tau)\rangle. \tag{B27}$$

The utility of the cross correlation is that it is affected by both the separations of the two sources and the size of each source. For example, the time lag at which the CCF maximizes is determined by the separation of the sources and by the effective velocity, $\mathbf{V}_{\rm eff}$ (Eq. 10,A18).

The cross correlation simplifies greatly if we assume that the amplitude-modulated noise in each source is statistically independent from the other. For pulsars, this is a reasonable assumption in many cases, though in others where there are drifting subpulse fluctuations that appear successively in different pulse components, this is an approximation. Letting $I_{1,2}$ be the (ensemble) mean intensity of each source, we find that

$$\begin{aligned} C_{\overline{\mathrm{I}}_{12}}(\mathbf{b},\overline{\tau}) &\equiv I_1(t)I_2(t+\overline{\tau}) \\ &+ \int\int d\mathbf{r_{s}}_1 d\mathbf{r_{s}}_2 \langle A(\mathbf{r_{s}}_1,t)\rangle\langle A(\mathbf{r_{s}}_2,t+\overline{\tau})\rangle\langle \gamma_G(\mathbf{b},\tau'+\overline{\tau},\delta\nu,\mathbf{r_{s}}_2-\mathbf{r_{s}}_1)\rangle_{\tau',T;\delta\nu,B}. \end{aligned} \tag{B28}$$

For two point sources, one at $\mathbf{r_{s}}_1$, another at $\mathbf{r_{s}}_2$, that have stationary statistics, the normalized crosscovariance is

$$\gamma_{\overline{\mathrm{I}}_{12}}(\mathbf{b},\overline{\tau}) \equiv \frac{C_{\overline{\mathrm{I}}_{12}}(\mathbf{b},\overline{\tau})-I_1I_2}{I_1I_2} = \left\langle \gamma_G(\mathbf{b},\tau'+\overline{\tau},\delta\nu,\mathbf{r_{s}}_2-\mathbf{r_{s}}_1)\right\rangle_{\tau',T;\delta\nu,B}. \tag{B29}$$

To illustrate the utility of the crosscovariance consider the case where γ_G is constant over the averaging intervals T and B. The time lag that maximizes $\gamma_{\overline{\mathrm{I}}_{12}}$ is the solution of

$$\frac{\partial}{\partial\overline{\tau}} D_\phi(\mathbf{b},\tau'+\overline{\tau},\mathbf{r_{s}}_2-\mathbf{r_{s}}_1) = 0. \tag{B30}$$

For a thin screen this becomes (c.f. Eq. 6-7)

$$\frac{\partial}{\partial \overline{\tau}} \left| \left(\frac{D_s}{d} \right) \mathbf{b} + \mathbf{V}_{\rm eff} \overline{\tau} + \left(\frac{D}{d} \right) \delta \mathbf{r_s} \right| = 0, \tag{B31}$$

which has the solution

$$\tau_{\rm max} = - \frac{\mathbf{V}_{\rm eff} \cdot [(D_s/d)\mathbf{b} + (D/d)\delta \mathbf{r_s}]}{{\rm V_{eff}}^2}. \tag{B32}$$

The ability to estimate $\tau_{\rm max}$ with precision depends on its value relative to the characteristic DISS time, which is the width of $\gamma_{\rm G}$ as a function of $\overline{\tau}$. Defining $\Delta t_{\rm d}$ using $\gamma_{\rm G}(0, \Delta t_{\rm d}, 0, 0) = e^{-1}$, we find that $\Delta t_{\rm d} = \ell_d / {\rm V_{eff}}$, where ℓ_d is the characteristic diffraction scale, yielding

$$\frac{\tau_{\rm max}}{\Delta t_{\rm d}} = - \frac{\mathbf{V}_{\rm eff} \cdot [(D_s/d)\mathbf{b} + (D/d)\delta \mathbf{r_s}]}{\ell_d {\rm V_{eff}}}. \tag{B33}$$

For $\mathbf{b} = 0$, we expect to identify $\delta \mathbf{r_s} \neq 0$ only if $(D/d)\delta \mathbf{r_s}$ is a sizable fraction of ℓ_d and also if the effective velocity is not orthogonal to $\delta \mathbf{r_s}$. The definition of 'sizable' depends on the number of independent ISS fluctuations used in any estimate of the cross correlation function, which is $N_{\rm ISS}$ given by Eq. 17. The error on $\tau_{\rm max} \sim \Delta t_{\rm d} {N_{\rm ISS}}^{-1/2}$, so a three-sigma measurement requires $\delta \mathbf{r}_{\mathbf{s}\parallel} \gtrsim 3 {N_{\rm ISS}}^{-1/2} (d \ell_d / D)$, where $\mathbf{r}_{\mathbf{s}\parallel} \equiv \mathbf{r_s} \cdot \mathbf{V}_{\rm eff}$.

Smirnova, Shishov & Malofeev (1996) give a similar expression for $\tau_{\rm max}$ that is based on a medium with a square-law structure function. Our result is more general.

C. Probability Densities for Strong Scattering

Here we derive probability density functions for the DISS gain in strong scattering. We use an exact treatment based on Karhunen-Loève expansions that take into account source extent and time-bandwidth averaging. Then we derive the PDF for the visibility and intensity that takes into account all features of the amplitude modulated noise model of Appendix A.

C.1. Exact Solution for the PDF of the Scintillation Gain

The time average intensity may be written as

$$\overline{\mathrm{I}}(\mathbf{r},t) = T^{-1}\int_{t\pm T/2} dt' \int d\mathbf{r_s}\, I_s(\mathbf{r_s})\, |\overline{g}(r,t',\nu,\mathbf{r_s})|^2 \tag{C1}$$

for a source with arbitrary brightness distribution I_s modulated by DISS. The DISS modulation $\overline{g}$ has been bandwidth averaged in accord with the considerations of Appendix A,

$$\overline{g}(\mathbf{r},t,\nu,\mathbf{r_s}) = B^{-1}\int_{\nu\pm B/2} d\nu'\, g(\mathbf{r},t,\nu',\mathbf{r_s}). \tag{C2}$$

Following the approach described by Goodman (1985; pp. 250-252), we expand $I_s^{1/2}(\mathbf{r_s})\overline{g}(\mathbf{r},t,\nu,\mathbf{r_s})$ onto a set of orthonormal basis vectors $\psi_n(t,\mathbf{r_s})$ with coefficients b_n. The orthonormality condition is

$$T^{-1}\int_{t\pm T/2} dt \int d\mathbf{r_s}\, \psi_n(t,\mathbf{r_s})\psi^*_{n'}(t,\mathbf{r_s}) = \delta_{nn'} \tag{C3}$$

and the b_n are given by

$$b_n = T^{-1}\int_{t\pm T/2} dt \int d\mathbf{r_s}\, I_s^{1/2}(\mathbf{r_s})\overline{g}(\mathbf{r},t,\nu,\mathbf{r_s})\psi_n(t,\mathbf{r_s}). \tag{C4}$$

By requiring that $\langle b_n b^*_{n'}\rangle = \langle |b_n|^2\rangle \delta_{nn'}$ (i.e. that the b_n are statistically independent), the following eigenvalue problem results:

$$(TB)^{-1}\int_{t-T/2}^{t+T/2} dt' \int_{-B}^{+B} d\delta\nu \left(1-\frac{|\delta\nu|}{B}\right)\int d\mathbf{r_{s1}}\, [I_s(\mathbf{r_{s1}})I_s(\mathbf{r_{s2}})]^{1/2}$$
$$\gamma_{\mathrm{g}}(0,t''-t',\delta\nu,\mathbf{r_{s2}}-\mathbf{r_{s1}})\psi_n(t',\mathbf{r_{s1}}) = \lambda_n\psi_n(t',\mathbf{r_{s2}}), \tag{C5}$$

where $\lambda_n = \langle |b_n|^2\rangle$ are the eigenvalues. The time and frequency averaging are handled differently because the wave propagator, g, is integrated over frequency before squaring of the wavefield, while time-averaging occurs after squaring.

The expansion implies that

$$\overline{\mathrm{I}}(\mathbf{r},t) = \sum_n |b_n|^2 \tag{C6}$$

and that

$$\langle I(\mathbf{r},t)\rangle = \sum_n \lambda_n. \tag{C7}$$

The expansion coefficients are gaussian distributed because the integral Eq. C4 is a sum of gaussian variables. Therefore, each term in Eq. C6, $|b_n|^2$, is exponentially distributed and the intensity PDF is the convolution of each of these exponentials.

The convolution can be calculated through Fourier transforms and inverted using the residue theorem yielding, for nondegenerate eigenvalues,

$$f_I(I) = \sum_{n=1}^{N} c_n\, e^{-I/\lambda_n} U(I), \tag{C8}$$

where $U(I)$ is the unit step function and the coefficients are given by

$$c_n = {\lambda_n}^{-1} \prod_{n' \neq n}^{N} \left(1 - \lambda_{n'}/\lambda_n\right)^{-1}. \tag{C9}$$

When only one eigenvalue is important, as it is for a point source with negligible time-bandwidth averaging, the PDF for I contains only a single term with mean $\lambda = \langle \mathrm{I} \rangle$.

C.2. Visibility PDF for the AMN Model

Here we present an alternative derivation of the visibility PDF that takes into account all source, propagation and additive-noise fluctuations.

The visibility function is the product of the narrowband fields from two sites (i and j)[4],

$$\Gamma(t) = \varepsilon_i(t)\varepsilon_j^*(t), \tag{C10}$$

where $\varepsilon_{i,j} = g_{i,j} a\, m + n_{i,j}$ for a point source that produces an identical field at the two sites. The propagator and the additive noise are both different at the two sites, in general.

The instantaneous value of the visibility is

$$\Gamma = g_i g_j^* A\, M + n_i n_j^* + a(g_i m n_j^* + g_j^* m^* n_i). \tag{C11}$$

We have simplified the notation, using i, j to label spatial location rather than using location and baseline vectors as we have used in previous sections. The first term is the scintillated pulsar signal, the second is due to additive noise at the two sites, while the third term represents cross

[4]We take the product at the same time in order to keep notation simple. In practice, a delay must be introduced to account for the different optical path lengths to the two sites. Our notation assumes this has already been removed.

products. If there were no scintillations, the visibility would be a noisy phasor (from the pulsar) combined with complex noise. Scintillations modify the source phasor to make it complex, in general. However, the pulsar noise (from A and M) are in phase with respect to the scintillations.

The (ensemble-average) mean visibility is

$$\langle \Gamma \rangle = \langle g_i g_j^* \rangle \langle A \rangle + \langle N_i \rangle \delta_{ij}. \tag{C12}$$

In practice, a time average is used to approximate the ensemble average, with attendant errors. We use the following notation for the time-averaged visibility:

$$\overline{\Gamma} = \langle \Gamma(t) \rangle_{BT} \equiv T^{-1} \int_{t-T/2}^{t+T/2} \Gamma(t), \tag{C13}$$

where the subscript 'BT' on the angular brackets denotes time averaging of a bandlimited process with bandwidth B.

By expanding A and M into mean values and zero-mean fluctuations, e.g. $A = \langle A \rangle + \delta A$ and $M = \langle M \rangle + \delta M$, we can write the time-average visibility as

$$\overline{\Gamma} = \langle g_i g_j^* \rangle_{BT} \langle \mathrm{A} \rangle \langle \mathrm{M} \rangle + \langle \mathrm{N}_i \rangle \delta_{ij} + X + C, \tag{C14}$$

where δ_{ij} is the Kronecker delta. The first term is due to the source, the second term is the mean system noise for a single site observation ($i = j$), and the last two terms are fluctuations,

$$\begin{aligned} X &= \langle g_i g_j^* \left[\delta A + \delta M \langle \mathrm{A} \rangle + \delta A \delta M \right] \rangle_{BT} \\ C &= \langle a (g_i m n_j^* + g_j^* m^* n_i) \rangle_{BT} + \langle n_i n_j^* \rangle_{BT} - \langle \mathrm{N}_i \rangle \delta_{ij}. \end{aligned}$$

We separate X and C because in useful limiting cases, discussed in the next subsections, they become, respectively, real and complex processes. For $i = j$, C also becomes real. Moreover, X is in phase with the phasor term, $\langle g_i g_j^* \rangle_{BT} \langle \mathrm{A} \rangle \langle \mathrm{M} \rangle$, while C is randomly phased.

If there are no intrinsic fluctuations, X vanishes and C then depends only on additive noise. However, the AMN model demands that there be source fluctuations even if there are no amplitude modulations. We let $\langle \mathrm{M} \rangle \equiv \langle |m|^2 \rangle = 1$ without any loss of generality.

Though we have assumed a point source to arrive at Eq. C14, the equation also applies to extended sources that are spatially incoherent. Spatial incoherence yields summation of contributions from different source elements that also imply Gaussian statistics.

All terms in X and C are uncorrelated, so variances of individual terms sum to yield the total variance. We assume time-bandwidth averaging such that $BT \gg 1$; thus X and C become Gaussian random variables (GRVs) by the Central Limit Theorem. However, we assume BT is small enough so that the DISS factor, $\langle g_i g_j^* \rangle_{BT}$, is not a GRV. For now, holding $g_i(t)$ and $g_j(t)$ as

fixed realizations of the DISS fluctuation (i.e. not averaging over an ensemble for these quantities), we find that X has PDF [5], $N(0,{\sigma_X}^2)$, while C has PDF $N_c(0,{\sigma_C}^2)$, where the variances are

$$ {\sigma_X}^2 = \langle |X|^2 \rangle = \langle \mathrm{A} \rangle^2 \langle G_i G_j \rangle_{BT} \, (BT)^{-1} \left[B \, W_A m_A^2 + m_M^2 (1 + m_A^2) \right] \tag{C15} $$

$$ {\sigma_C}^2 = \langle |C|^2 \rangle = (2\,BT)^{-1} \left[\langle \mathrm{A} \rangle \left(\langle \mathrm{N}_i \rangle \langle G_j \rangle_{BT} + \langle \mathrm{N}_j \rangle \langle G_i \rangle_{BT} \right) + \langle \mathrm{N}_i \rangle \langle \mathrm{N}_j \rangle \right], \tag{C16} $$

and we have used $G_i \equiv |g_i|^2$, etc. The forms of these variances are consistent with expressions given by Rickett (1975). In general, we can write the variances of the real and imaginary parts of X and C as $\sigma^2_{X_{r,i}} = \frac{1}{2}\sigma^2_X(1 \pm \rho_{G_{i,j}})$ and $\sigma^2_{C_{r,i}} = \frac{1}{2}\sigma^2_C(1 \pm \delta_{i,j})$. When the DISS is perfectly correlated between the two sites, the correlation coefficient $\rho_{G_{i,j}}$ (which is equal to $\gamma_\mathrm{G}(\mathbf{b}, 0, 0, 0)$, c.f. Eq. A19) is unity and X is real. As the DISS decorrelates between the sites, the $\sigma_{X_i} \rightarrow \sigma_{X_r}$. Only when the two sites are identical (e.g. for a single aperture measurement of intensity) is C real. For all interferometers, C is complex with equal variances of the real and imaginary parts.

Deriving the variances involves assumptions about the correlation times for the various signal terms and how they influence mean squares of the time averages. We have assumed that n and m, the noise processes, have correlation times much smaller than that of the amplitude modulation, a, which in turn has a much smaller correlation time than the integration time used. This hierarchy is consistent with the fact that the noise correlation times are the reciprocal of the bandwidth used. For pulsars, data are often obtained by using only a small range of pulse phase but averaging over many pulse periods. Pulsar pulses are broad band but decorrelate on times about equal to the spin period. Our expression for σ_X uses the correlation time W_A for the amplitude modulation. This is effectively the width of the correlation function ρ_A defined in Eq. B2. As applied in Paper II, we would take W_A to be the width, $\Delta t \equiv P \Delta\phi_p$, of the pulse window used in the analysis, where P is the pulse phase and $\Delta\phi_p$ is the window width in pulse phase units (cycles). Then $T = N_p \Delta t$. We have also included m_M, the modulation index of pulsar noise fluctuations. For amplitude modulated noise with Gaussian statistics, $m_M \equiv 1$. By retaining it, we can see what changes in the statistics if we artifically turn off the noise fluctuations. σ_C depends on $\langle \mathrm{M} \rangle$ but not on m_M.

Note that the contribution of pulsar noise to visibility fluctuations relative to the contribution from additive noise is independent of the averaging time. Consider, for example, the ratio σ_X/σ_+, where σ_+ is the value of σ_C when there is no source. We have $\sigma_X/\sigma_+ \propto \mathrm{SNR}_0$, where $\mathrm{SNR}_0 \equiv \langle \mathrm{A} \rangle / \sqrt{\langle \mathrm{N}_i \rangle \langle \mathrm{N}_j \rangle}$ is the ratio of source strength to system temperature, when both are in the same units (e.g. Janskys). Similarly, $\sigma_C/\sigma_+ - 1 \propto \sqrt{\mathrm{SNR}_0}$. This result is at odds with Gwinn *et al.* (2000), who state that pulsar "self noise" can be ignored because it diminishes with averaging time. It does diminish but it cannot be ignored unless the signal to noise ratio is small.

The PDF for $\overline{\Gamma}$ given $g_i(t)$ and $g_j(t)$ may be calculated by appropriate integration over the Gaussian PDFs for X and C. We now consider some specific cases.

---

[5] $N(0,{\sigma_X}^2)$ denotes a Gaussian PDF of a real variable with zero mean and variance ${\sigma_X}^2$ while $N_\mathrm{c}(0,{\sigma_C}^2)$ denotes a complex Gaussian quantity having real and imaginary parts with equal variances, ${\sigma_C}^2$.

C.3. DISS Perfectly Correlated Between Sites and Constant over BT

For perfectly correlated DISS (between sites i and j), $\langle g_i g_j^* \rangle_{BT} \rightarrow \langle G_i \rangle_{BT} = \langle G_j \rangle_{BT} \equiv \langle G \rangle_{BT}$ and $\langle G_i G_j) \rangle_{BT} \rightarrow \langle G^2 \rangle_{BT}$; thus X becomes real. If, moreover, the DISS modulation is constant over the averaging time T, then $\langle G \rangle_{BT} \rightarrow G =$ constant and $\langle G^2 \rangle_{BT} \rightarrow G^2$. The visibility becomes

$$\overline{\Gamma} = G\langle \mathrm{A} \rangle + \langle \mathrm{N}_i \rangle \delta_{ij} + X + C. \tag{C17}$$

We assume a point source (and strong, saturated scintillations) so that, with G constant over T, the scintillation PDF is a one-sided exponential. The PDFs of individual elements of $\overline{\Gamma}$ are

$$\begin{aligned} f_G(G) &= e^{-G} U(G) \\ f_X(X) &= N(0, {\sigma_X}^2) \\ f_C(C) &= N_c(0, {\sigma_C}^2) \\ {\sigma_X}^2 &= G^2 \langle \mathrm{A} \rangle^2 (BT)^{-1} \left[B\, W_A m_A^2 + m_M^2 (1 + m_A^2) \right] \\ {\sigma_C}^2 &= (2\,BT)^{-1} \left[(\langle \mathrm{N}_i \rangle \langle \mathrm{N}_j \rangle) + + G\langle \mathrm{A} \rangle (\langle \mathrm{N}_i \rangle + \langle \mathrm{N}_j \rangle) \right]. \end{aligned} \tag{C18}$$

C.3.1. PDF of the Complex Visibility

Let $\overline{\Gamma} = \overline{\Gamma}_r + i\overline{\Gamma}_i$. The PDF of $\overline{\Gamma}$ is

$$\begin{aligned} f_{\overline{\Gamma}}(\overline{\Gamma}) &= \int dG\, f_G(G) \int dX f_X(X) f_C(\overline{\Gamma}_r - G\langle \mathrm{A} \rangle - X, \overline{\Gamma}_i) \\ &= \int dG\, f_G(G) \int dX (2\pi\sigma_X)^{-1/2} e^{-X^2/2\sigma_X^2} (2\pi\sigma_C)^{-1} e^{-\frac{1}{2\sigma_C^2}\left[(\overline{\Gamma}_r - G\langle \mathrm{A} \rangle - X)^2 + \overline{\Gamma}_i^2 \right]} \end{aligned} \tag{C19}$$

Performing the integral over X, we obtain

$$f_{\overline{\Gamma}}(\overline{\Gamma}) = (2\pi\sigma_C)^{-1} e^{-\overline{\Gamma}_i^2/2\sigma_C^2} \int dG\, f_G(G) (\sigma_X^2 + \sigma_C^2)^{-1/2} e^{-\frac{1}{2}(\overline{\Gamma}_r - G\langle \mathrm{A} \rangle)^2 / 2(\sigma_X^2 + \sigma_C^2)}. \tag{C20}$$

Note that for no signal ($\langle \mathrm{A} \rangle \rightarrow 0$), we get

$$f_{\overline{\Gamma}}(\overline{\Gamma}) = (2\pi\sigma_C^2)^{-1} e^{-|\overline{\Gamma}|^2/2\sigma_C^2}, \tag{C21}$$

a circular Gaussian PDF. Our expression in Eq. C20 disagrees with Eq. 11 of Gwinn *et al.* (2000), which assigns equal variances to the real and imaginary parts of $\overline{\Gamma}$. The variances are not equal, in general. Also, there is an extra factor of 2π in their equation.

C.3.2. PDF of the Visibility Magnitude

The PDF of $|\overline{\Gamma}|$ can be calculated as

$$f_{|\overline{\Gamma}|}(|\overline{\Gamma}|) = |\overline{\Gamma}| \int_0^{2\pi} d\phi\, f_{\overline{\Gamma}}(|\overline{\Gamma}| \cos\phi, |\overline{\Gamma}| \sin\phi). \tag{C22}$$

Here we take a slightly different approach. It is convenient to scale the magnitude of the visibility by the rms of the complex term, σ_C. Using $\gamma \equiv |\overline{\Gamma}|/\sigma_C$ and $i \equiv \langle \mathrm{A} \rangle / \sigma_C$, the conditional PDF for constant G and $X = 0$ is

$$f_\gamma(\gamma|i, G) = \gamma e^{-\frac{1}{2}(\gamma^2 + G^2 i^2)} I_0(\gamma i), \tag{C23}$$

where I_0 is the modified Bessel function. This result is the well known Rice-Nakagami PDF for a real phasor of length i combined with a complex Gaussian phasor (e.g. Thomson, Moran & Swenson 1991, Eq. 9.37). Integrating over the PDF for X, we have, for fixed G,

$$f_\gamma(\gamma|G) = \int dX f_X(X) f_\gamma(\gamma|i + \frac{X}{G\sigma_C}, G). \tag{C24}$$

Then, integrating over the PDF for G, we have the PDF for γ that takes into account all fluctuations, including DISS,

$$f_\gamma(\gamma) = \int dG f_G(G) f_\gamma(\gamma|G). \tag{C25}$$

For $\mathrm{S/N} \to \infty$, $\sigma_C \to 0$,

$$\overline{\Gamma} \;=\; G\langle \mathrm{A} \rangle + \langle \mathrm{N}_i \rangle \delta_{ij} + X, \tag{C26}$$

and the PDF of $|\overline{\Gamma}|$ for fixed G becomes $N(G\langle \mathrm{A} \rangle + \langle \mathrm{N}_i \rangle \delta_{ij}, {\sigma_X}^2)$, with the PDF for γ given by Eq. C25.

C.4. Perfectly Correlated DISS but $G \neq$ Constant over BT

Specializing to the case of a weak source for which $\sigma_X \ll \sigma_C$, we have (using $G \equiv \langle G \rangle_{BT}$)

$$\overline{\Gamma} \;\approx\; G\langle \mathrm{A} \rangle + \langle \mathrm{N}_i \rangle \delta_{ij} + C$$

$$f_G(G) \;\approx\; \frac{(GN_{\mathrm{ISS}})^{N_{\mathrm{ISS}}}}{G\Gamma(N_{\mathrm{ISS}})} e^{-GN_{\mathrm{ISS}}} U(G),$$

where $\Gamma(x)$ is the gamma function and $U(x)$ is the unit step function. G is distributed approximately as $\chi^2_{2N_{\mathrm{ISS}}}$, a chi-square random variable with $2N_{\mathrm{ISS}}$ degrees of freedom, where $N_{\mathrm{ISS}} \equiv m_{\mathrm{ISS}}^{-2}$ and where m^2_{ISS} is given by Eq. 17. The true PDF of G is obtained by solving the appropriate Fredholm equation for the eigenvalues that determine the PDF, as described in the main text.

REFERENCES

Armstrong, J. W., Spangler, S. R., & Hardee, P. E. 1977, AJ, 82, 785

Armstrong, J. W., Rickett, B. J. & Spangler, S. R. 1995, ApJ, 443, 209

Backer, D. C. 1975, A&A, 43, 395

Barnard, J. J. & Arons, J. 1986, ApJ, 302, 138

Bartel, N. & Hankins, T. H. 1982, ApJ, 254, L35

Blaskiewicz, M., Cordes, J. M. & Wasserman, I. 1991, ApJ, 370, 643

Charnotskii, M. I., Myakinin, V. A. & Zavorotnyy, V. U. 1990, J. Opt. Soc. Am. A., 7, 1345

Chashei, I. V. & Shishov, V. I. 1976, AZh, 53, 26.

Condon, J. J. & Backer, D. C. 1975, ApJ, 197, 31

Condon, J. J. & Dennison, B. 1978, ApJ, 224, 835

Cordes, J. M. 1976a, ApJ, 208, 944

Cordes, J. M. 1976b, ApJ, 210, 780

Cordes, J. M. 1986, ApJ, 311, 183

Cordes, J. M. & Hankins, T. H. 1979, ApJ, 233, 981

Cordes, J. M., Weisberg, J. M. & Boriakoff, V. 1983, ApJ, 268, 370

Cordes, J. M., Pidwerbetsky, A. & Lovelace, R. V. E. 1986, ApJ, 310, 737

Cordes, J. M. & Lazio, T. J. W. 1991, ApJ, 376, 123

Cordes, J. M. & Rickett, B. J. 1998, ApJ, 507, 846

Cornwell, T. J. & Narayan, R. 1993, ApJ, 408, L68

Dennison, B. & Condon, J. J. 1981, ApJ, 246, 91

Desai, K. M., Gwinn, C. R. *et al.* 1992, ApJ, 393, L75

Desai, K. & Gwinn, C. 1998, Interstellar Turbulence, E6

Evans, N.J., Hills, R.E., Rydbeck, O. E. H. & Kollberg, E. 1972, Phys. Rev., A, 6, 1643-1647

Frail, D. A., Diamond, P. J., Cordes, J. M. & Van Langevelde, H. J. 1994, ApJ, 427, L43

Frail, D. A., Kulkarni, S. R., NiCastro, S. R., Feroci, M., & Taylor, G. B. 1997, Nature, 389, 261.

Goodman, J. W. 1985, *Statistical Optics*, New York:Wiley

Goodman, J. 1997, NewA, 2, 449

Goodman, J. & Narayan, R. 1989, MNRAS, 238, 995

Gupta,Y., Rickett, B. J. & Lyne, A. G. 1994, MNRAS, 269, 1035

Gwinn, C. R. *et al.* 1997, ApJ, 483, L53

Gwinn, C. R. *et al.* 1998, ApJ, 505, 928

Gwinn, C. R. *et al.* 2000, ApJ, 531, 902

Hankins, T. H. & Boriakoff, V. 1981, ApJ, 249, 238

Hanbury Brown, R. 1974, *The Intensity Interferometer*, New York: Wiley.

Kuzmin, O. A. 1992 in *The Magnetospheric Structure and Emission Mechanisms of Radio Pulsars*, Proceedings IAU Colloq. 128, Eds. T. H. Hankins, J. M. Rankin & J. A. Gil, Zielona Góra, Poland: Pedagogical University Press, pp. 287-289

Lambert, H. & Rickett, B. J. 1999, ApJ, 517, 299

Gregory, P. C. & Loredo, T. J. 1992, ApJ, 398, 146.

Lotova, N. A. & Chashei, I. V. 1981, Sov. Ast, 25, 309

Lovelace, R.V.E. 1970, PhD Thesis, Cornell University

Molnar, L. A., Mutel, R. L., Reid, M. J. & Johnston, K. J. 1995, ApJ, 438, 708

Moran, J. M. 1981, BAAS, 13, 508

Press, W.H., Teukolsky, S. A., Vetterling, W. T. & Flannery, B. P. 1992, Numerical Recipes, Second Edition, Cambridge University Press

Rickett, B. J. 1975, ApJ, 197, 185

Rickett, B. J. 1990, ARA&A, 28, 561

Smirnova, T. V., Shishov, V. I., & Malofeev, V. M. 1996, ApJ, 462, 289

Spangler, S. R. & Cordes, J. M. 1998, ApJ, 505, 766

Thomas, J. B. 1969, Statistical Communication Theory, Wiley: New york.

Thompson, A. R., Moran, J. M. & Swenson, G. W. 1991, *Interferometry and Synthesis in Radio Astronomy*, Krieger Publishing Co: Malabar, Florida

Trotter, A. S., Moran, J. M. & Rodriguez, L. F. 1998, ApJ, 493, 666

Yusef-Zadeh, F. , Cotton, W. , Wardle, M. , Melia, F. & Roberts, D. A. 1994, ApJ, 434, L63

Wilkinson, P. N., Narayan, R. & Spencer, R. E. 1994, MNRAS, 269, 67.

Wolszczan, A. & Cordes, J. M. 1987, ApJ, 320, L35

Table 1: Symbols and Acronyms Used

Symbols	Definition
$\langle \cdots \rangle$	Ensemble average
$\langle \cdots \rangle_{BT}$	Time average over time T of a process with bandwidth B
ACF	Autocorrelation function
CCF	Crosscorrelation function
DISS	Diffractive Interstellar Scintillation
DM	Dispersion Measure
RISS	Refractive Interstellar Scintillation
$a(t)$	Amplitude modulation (real)
$A = a^2$	Intensity modulation
B, $\Delta\nu$	Bandwidth
$\mathbf{b}$	Baseline
b_e	1/e scale of phase structure function
$b_{\rm eff}$	effective baseline
$C_{\rm I}$	Intensity CCF
C_n^2	Coefficient in electron-density wavenumber spectrum
d	Earth-source distance
$D = d - D_s$	Screen-Earth distance
D_s	Source-screen distance
D_ϕ	Phase structure function
f_α	Numerical factor in structure function
$f_G(G)$	PDF of scintillation modulation
$f_\gamma(\gamma)$	PDF of normalized visibility
g	Wave propagator
$G = \|g\|^2$	Scintillation modulation of intensity or scintillation "gain."
E_Δ	Narrowband electric field
ε	Complex baseband electric field
ε_s	Complex electric field at source
I	Intensity
δI	Intensity flucutation
$\overline{\rm I}$	Time-average intensity
$\mathcal{L}$	Likelihood function
ℓ_d	Characteristic spatial scale in diffraction pattern
$m(t)$	Complex gaussian noise with unit mean square
$M \equiv \|m\|^2$	Squared magnitude of m
m_A	Modulation index of A

Table 1: Symbols and Acronyms Used (continued)

Symbols	Definition
$m_{\rm ISS}$	Scintillation modulation index (= rms / mean)
m_M	Modulation index of M
$N_{\rm dof}$	Number of degrees of freedom in scintillations
$N_{\rm ISS}$	Number of independent scintillation features averaged
$n(t)$	Additive complex Gaussian noise
n_e	Free electron density
$R_{\overline{\rm I}}$	ACF of averaged intensity
$R_{\overline{\Gamma}}$	ACF of averaged visibility
$R_{4\varepsilon}$	Fourth moment of complex field
$\mathbf{r_s}$	Two dimensional vector at source
r_0	Fried scale
s	Location along line of sight, $s = 0$ at source
T	Integration or averaging time
τ_i	Time lag used in calculating interferometer visibilities
$\mathbf{V}_{\rm eff}$	Vector effective velocity
$V_{\rm obs}$	Observer's velocity
$V_{\rm p}$	Pulsar velocity
$V_{\rm m}$	Velocity of scattering medium
$V_{\rm ISS}$	Velocity of ISS diffraction pattern
α	Exponent in phase structure function
$\Gamma_{\rm I}$	Intensity autocovariance function
Γ_ε	Visibility function
$\overline{\Gamma}$	Time average of visibility function
$\gamma_{\rm g}$	Second moment of propagator g
$\gamma_{\rm G}$	autocovariance of scintillation 'gain' G
$\Delta(\tau)$	Normalized ACF of noise
$\Delta\nu_{\rm d}$	Diffraction or scintillation bandwidth
$\Delta t_{\rm d}$	Diffraction or scintillation time scale
ϕ	Phase perturbation from refractive index perturbations
ψ_n	Eigenfunction in Karhunen-Loève problem
ρ_A	Autocorrelation function of $A(t)$
b_{iso}	Isoplanatic scale of diffraction pattern at observer's location
$\delta r_{s,iso}$	Isoplanatic scale at source's location
σ_r	Length scale in Gaussian brightness distribution
θ_{iso}	Isoplanatic angle
θ_s	Source angular size

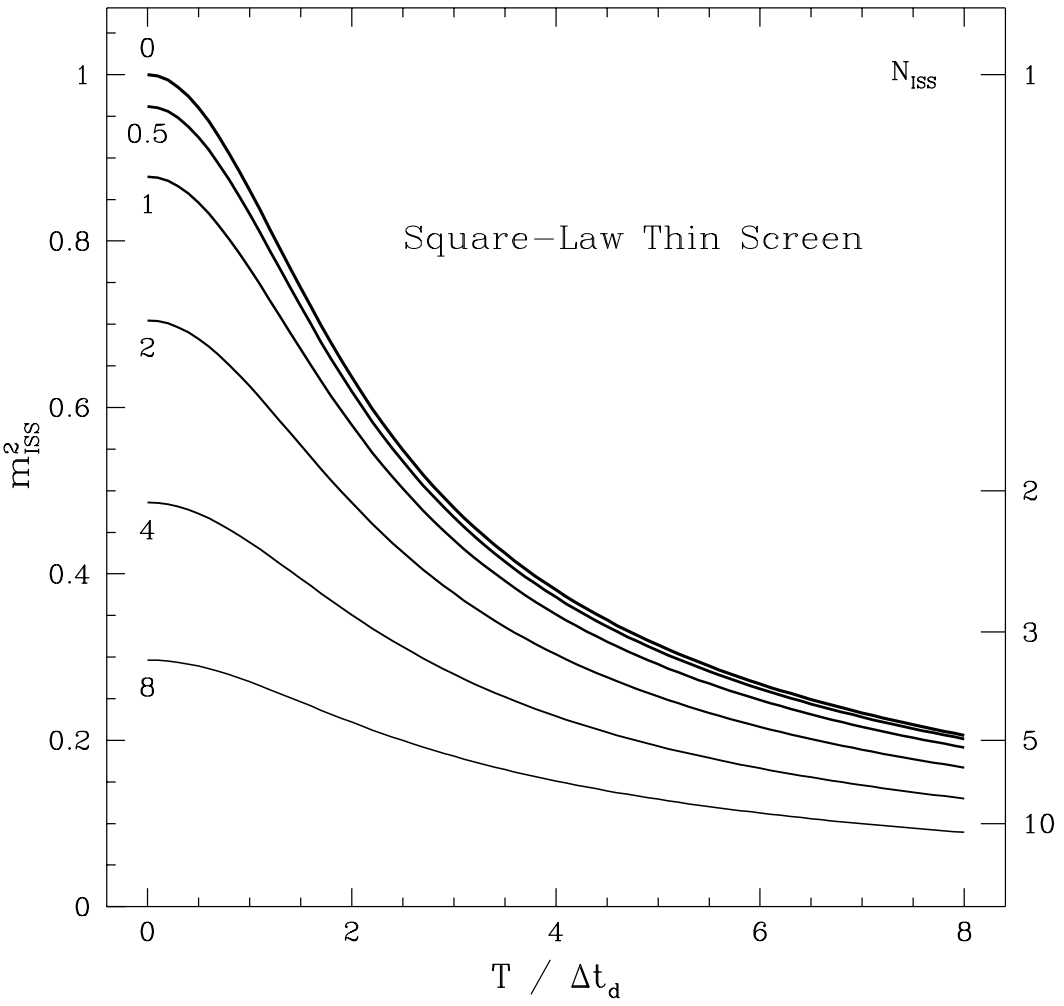

Fig. 1.— The DISS modulation index plotted against averaging time in units of the characteristic diffraction time, $T/\Delta t_{\rm d}$ for values of the frequency resolution in units of the characteristic diffraction bandwidth, $B/\Delta\nu_{\rm d} = 0, 0.5, 1, 2, 5, 10$. The right hand scale gives the effective number of ISS fluctuations that are averaged, $N_{\rm ISS} = 1/m^2_{\rm ISS}$. This case applies to a thin-screen having a square-law structure function.

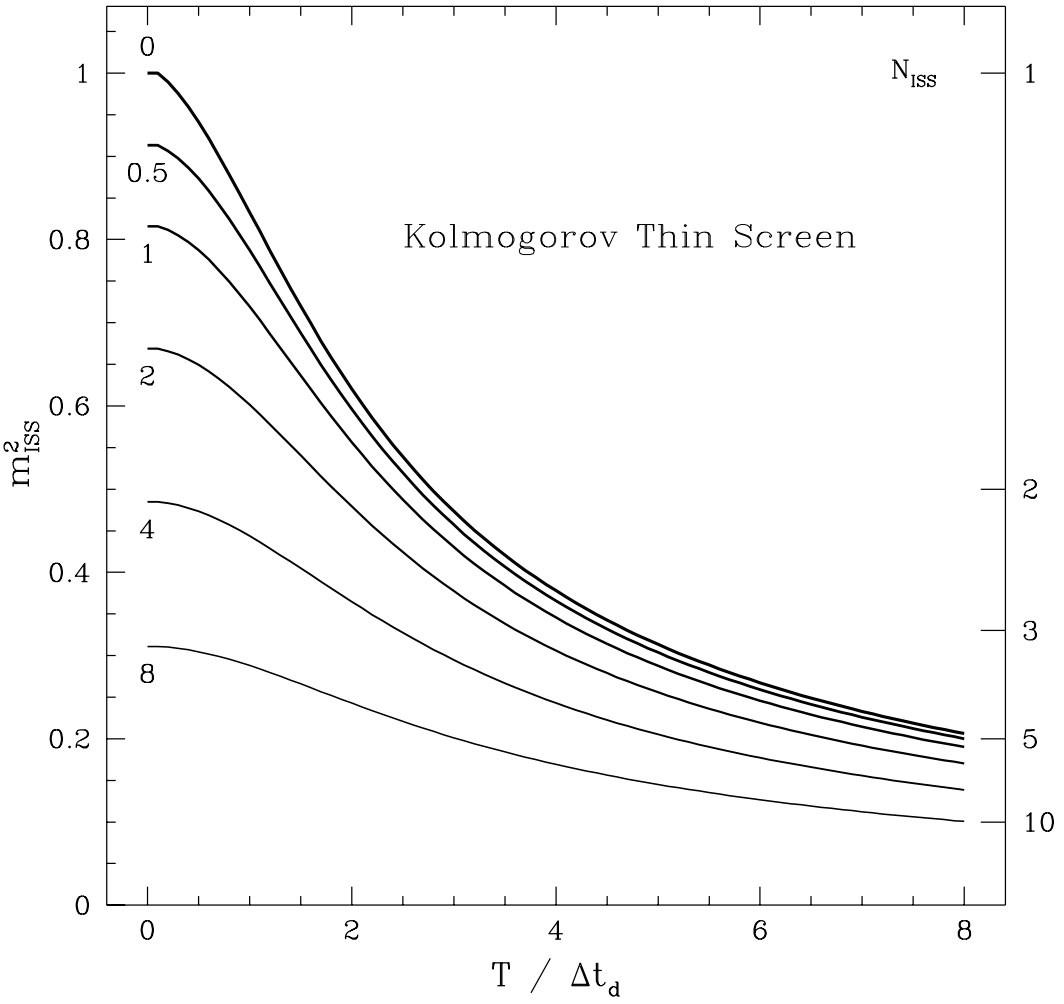

Fig. 2.— The DISS modulation index plotted against averaging time in units of the characteristic diffraction time, $T/\Delta t_{\rm d}$ for values of the frequency resolution B in units of the characteristic diffraction bandwidth, $B/\Delta\nu_{\rm d} = 0, 0.5, 1, 2, 4, 8,$ as labelled. This case is for a thin screen with a Kolmogorov wavenumber spectrum. The right-hand scale indicates the number of ISS fluctuations ('scintles') averaged, $N_{\rm ISS}$.

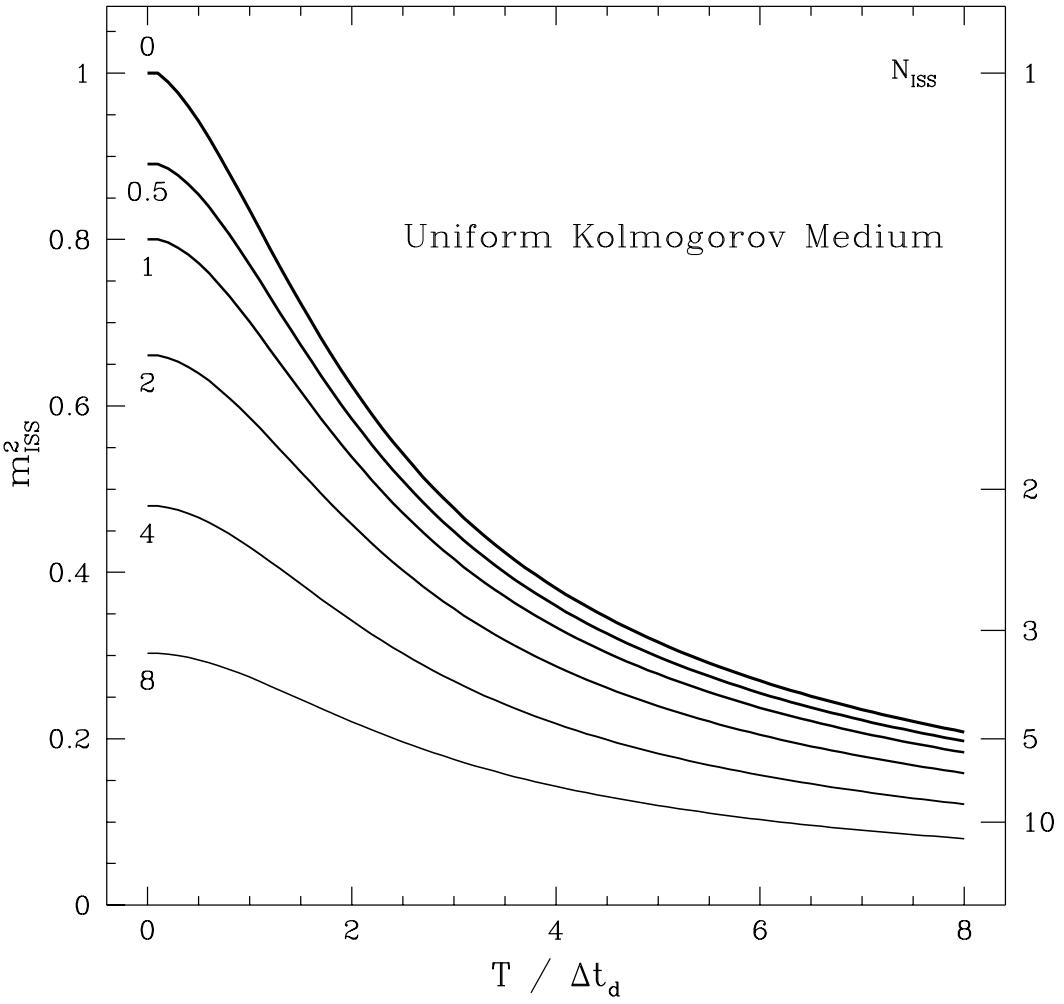

Fig. 3.— The DISS modulation index plotted against averaging time in units of the characteristic diffraction time, $T/\Delta t_{\rm d}$ for values of the frequency resolution B in units of the characteristic diffraction bandwidth, $B/\Delta\nu_{\rm d} = 0, 0.5, 1, 2, 4, 8$, as labelled. This case is for a uniform medium with a Kolmogorov wavenumber spectrum. The right-hand scale indicates the number of ISS fluctuations ('scintles') averaged, $N_{\rm ISS}$.

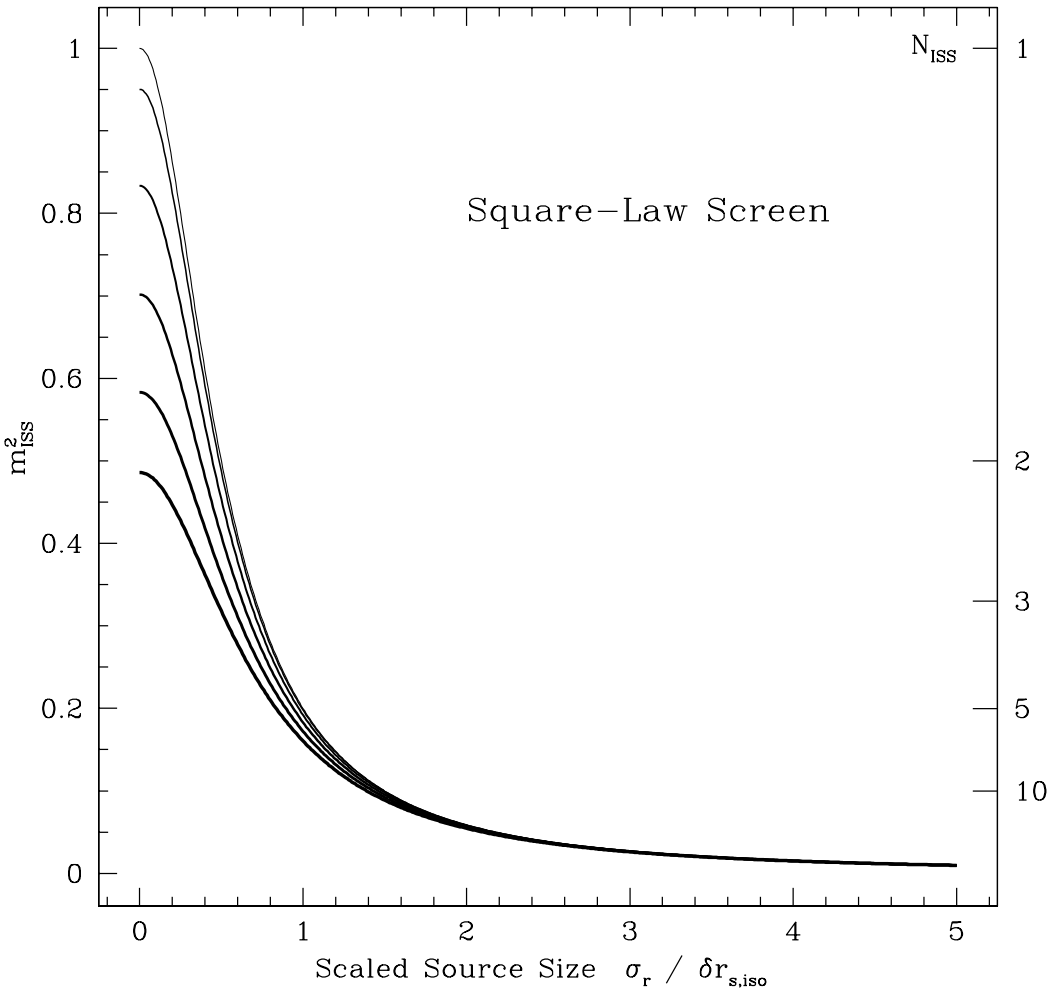

Fig. 4.— The DISS modulation index plotted against source size in units of the isoplanatic scale, $\delta r_{s,iso}$. The different curves are for different values of averaging time T and bandwidth B in units of the characteristic diffraction time scale and bandwidth. In order of light to heavy lines, the curves are $(T/\Delta t_{\rm d}, B/\Delta\nu_{\rm d}) = (0,0), (0.4,0.4), (0.8,0.8), (1.2,1.2), (1.6,1.6), (2.0,2.0)$. This case is for a thin screen with a square-law structure function. The right-hand scale indicates the number of ISS fluctuations ('scintles') averaged, $N_{\rm ISS}$.

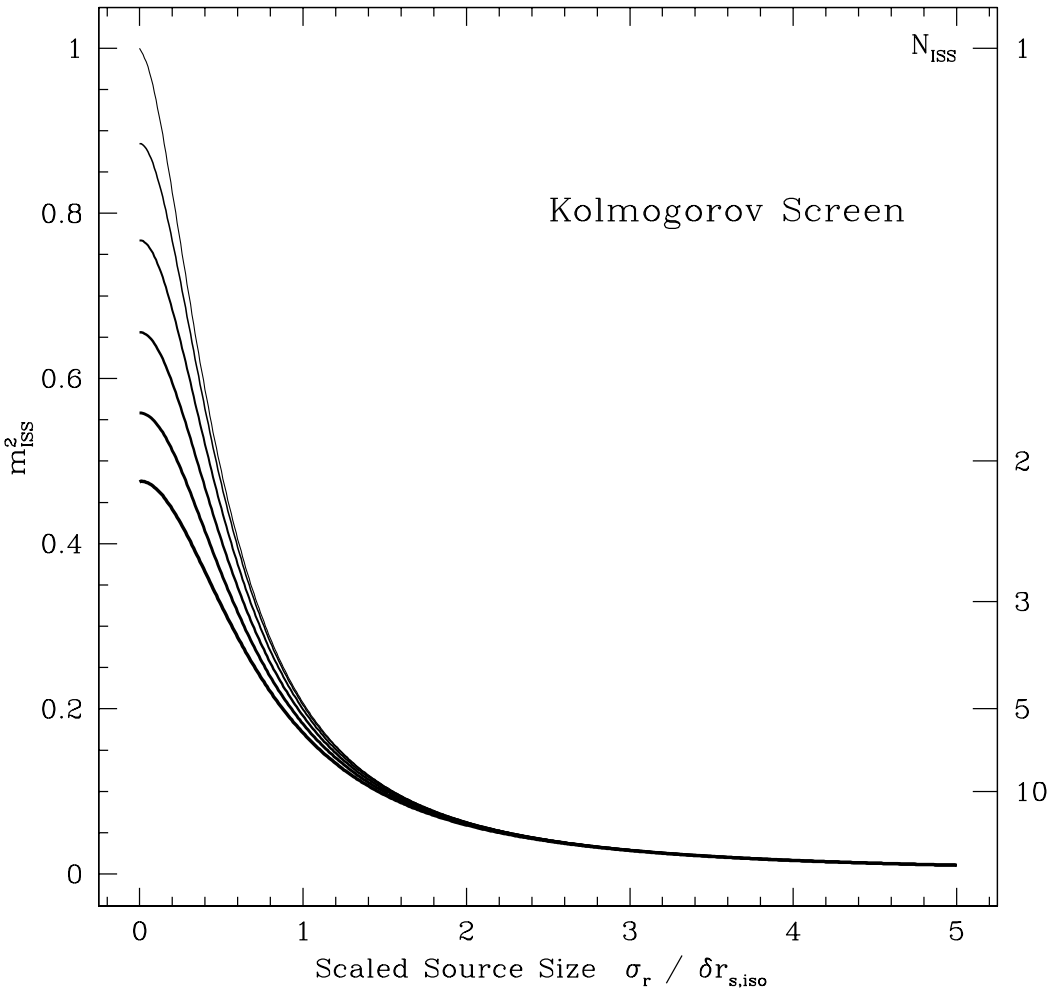

Fig. 5.— The DISS modulation index plotted against source size in units of the isoplanatic scale, $\delta r_{s,iso}$. The different curves are for different values of averaging time T and bandwidth B in units of the characteristic diffraction time scale and bandwidth. In order of light to heavy lines, the curves are $(T/\Delta t_{\rm d}, B/\Delta\nu_{\rm d}) = (0,0), (0.4,0.4), (0.8,0.8), (1.2,1.2), (1.6,1.6), (2.0,2.0)$. This case is for a thin screen with a Kolmogorov ($\alpha = 5/3$) structure function. The right-hand scale indicates the number of ISS fluctuations ('scintles') averaged, $N_{\rm ISS}$.

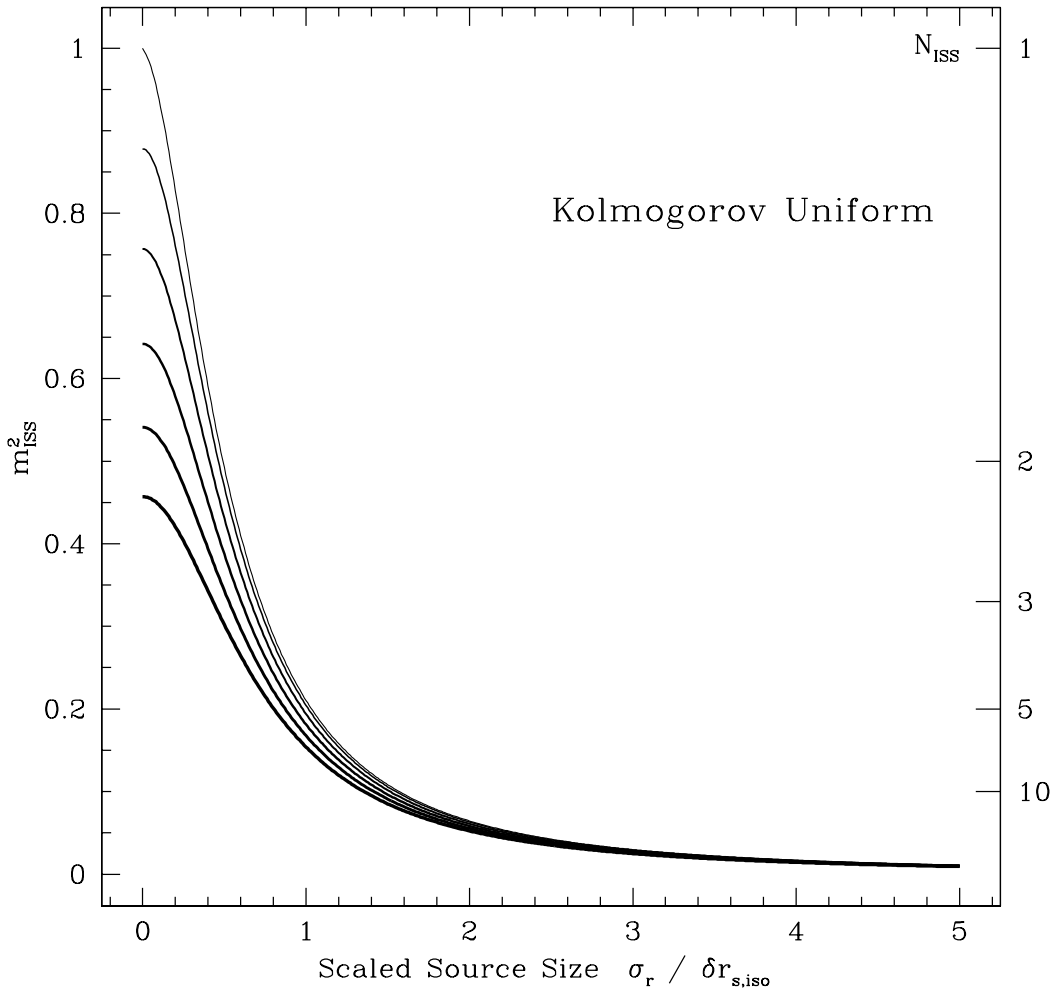

Fig. 6.— The DISS modulation index plotted against source size in units of the isoplanatic scale, $\delta r_{s,iso}$. The different curves are for different values of averaging time T and bandwidth B in units of the characteristic diffraction time scale and bandwidth. In order of light to heavy lines, the curves are $(T/\Delta t_{\rm d}, B/\Delta\nu_{\rm d}) = (0,0), (0.4,0.4), (0.8,0.8), (1.2,1.2), (1.6,1.6), (2.0,2.0)$. This case is for a uniformly extended medium with a Kolmogorov ($\alpha = 5/3$) structure function. The right-hand scale indicates the number of ISS fluctuations ('scintles') averaged, $N_{\rm ISS}$.

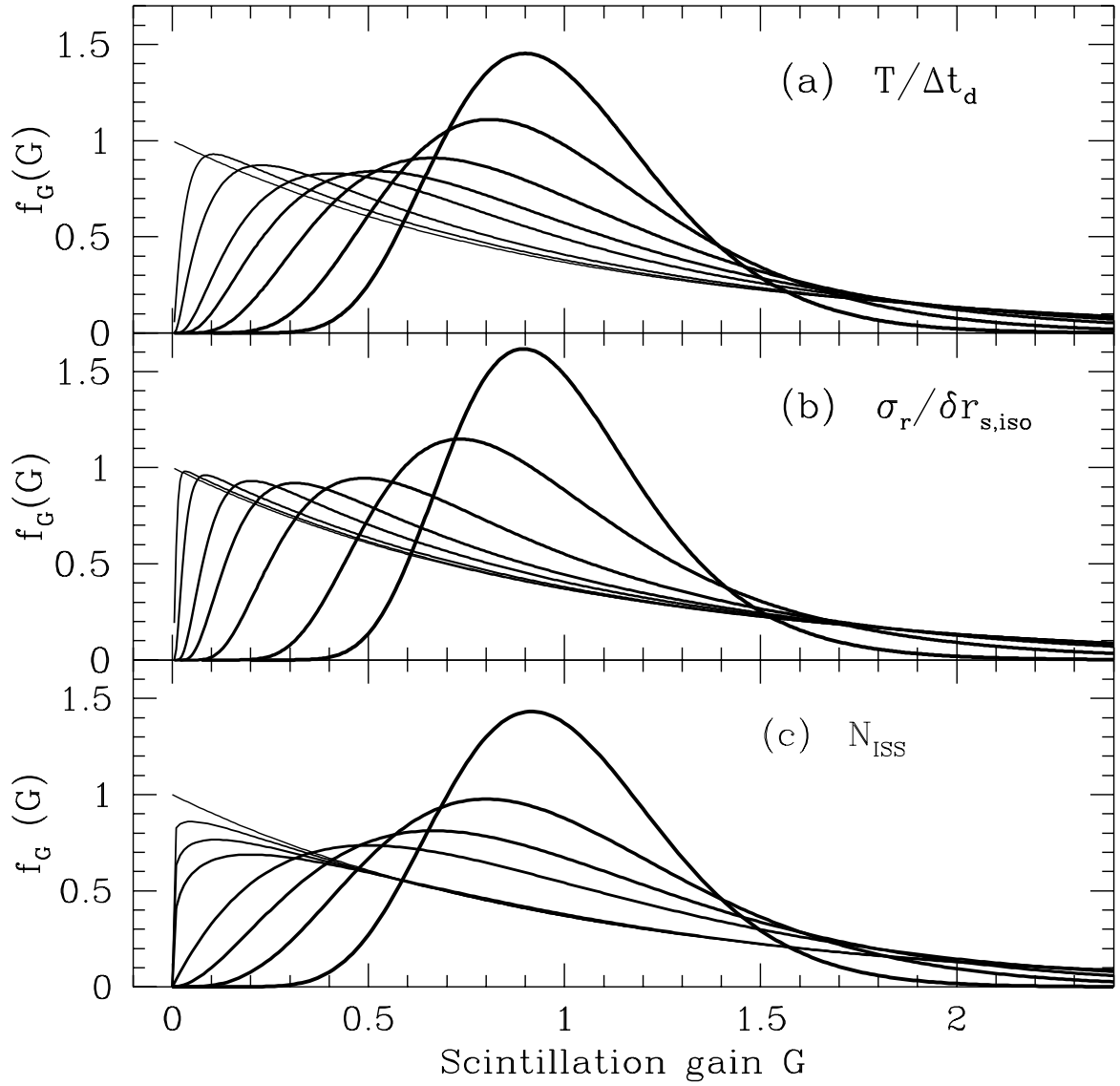

Fig. 7.— Probability density functions for the DISS 'gain' G for different amounts of time averaging and source extent. (a) PDFs vs. averaging time. The different curves going from thinnest to thickest lines are for $T/\Delta t_{\rm d}$ = 0.01, 0.5, 1, 2, 3, 5, 10 and 20. The PDFs were determined by solving a homogeneous Fredholm equation, as discussed in the text. (b) PDFs for Gaussian brightness distributions with different sizes relative to the isoplanatic size. The different curves going from thinnest to thickest lines are for $\sigma_r/\delta r_{s,iso}$ = 0.01, 0.05, 0.1, 0.2, 0.3, 0.5, 1.0 and 2. These curves were determined by solving a two-dimensional Fredholm equation. (c) Approximate PDFs given by a $\chi^2_{2N_{\rm ISS}}$ PDF with number of degrees of freedom $2N_{\rm ISS}$, where $N_{\rm ISS} = 1, 1.05, 1.125, 1.25, 2, 3, 5$ and 12.

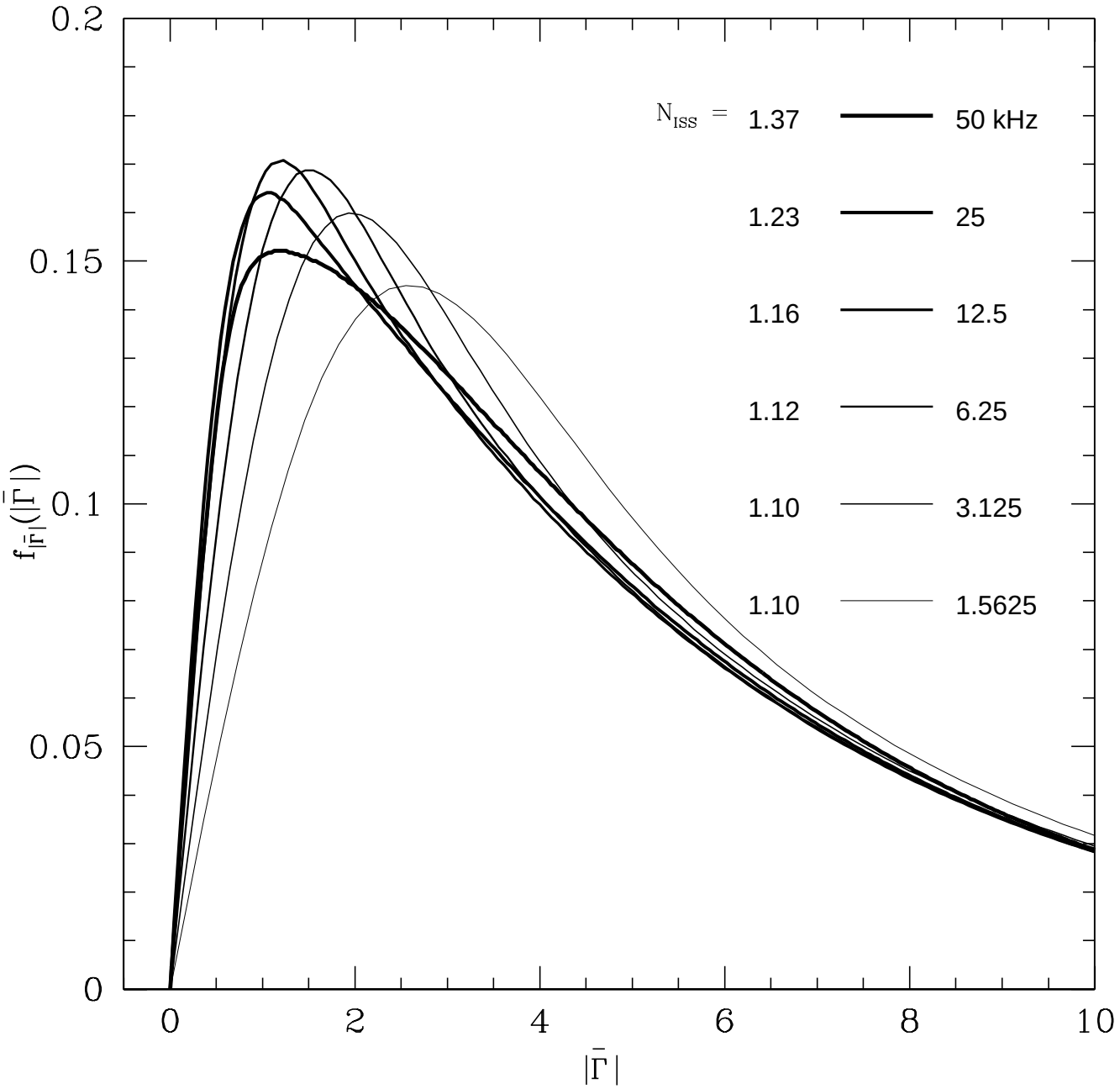

Fig. 8.— Probability density function for the visibility magnitude for different bandwidths for cases where $\langle A \rangle / \langle N \rangle = 0.14$. The different curves are for different bandwidths, as labelled, which correspond to different numbers of ISS fluctuations, also as labelled. This figure corresponds to cases where ISS variations and the complex term X are both included in Eq. C23-C25.

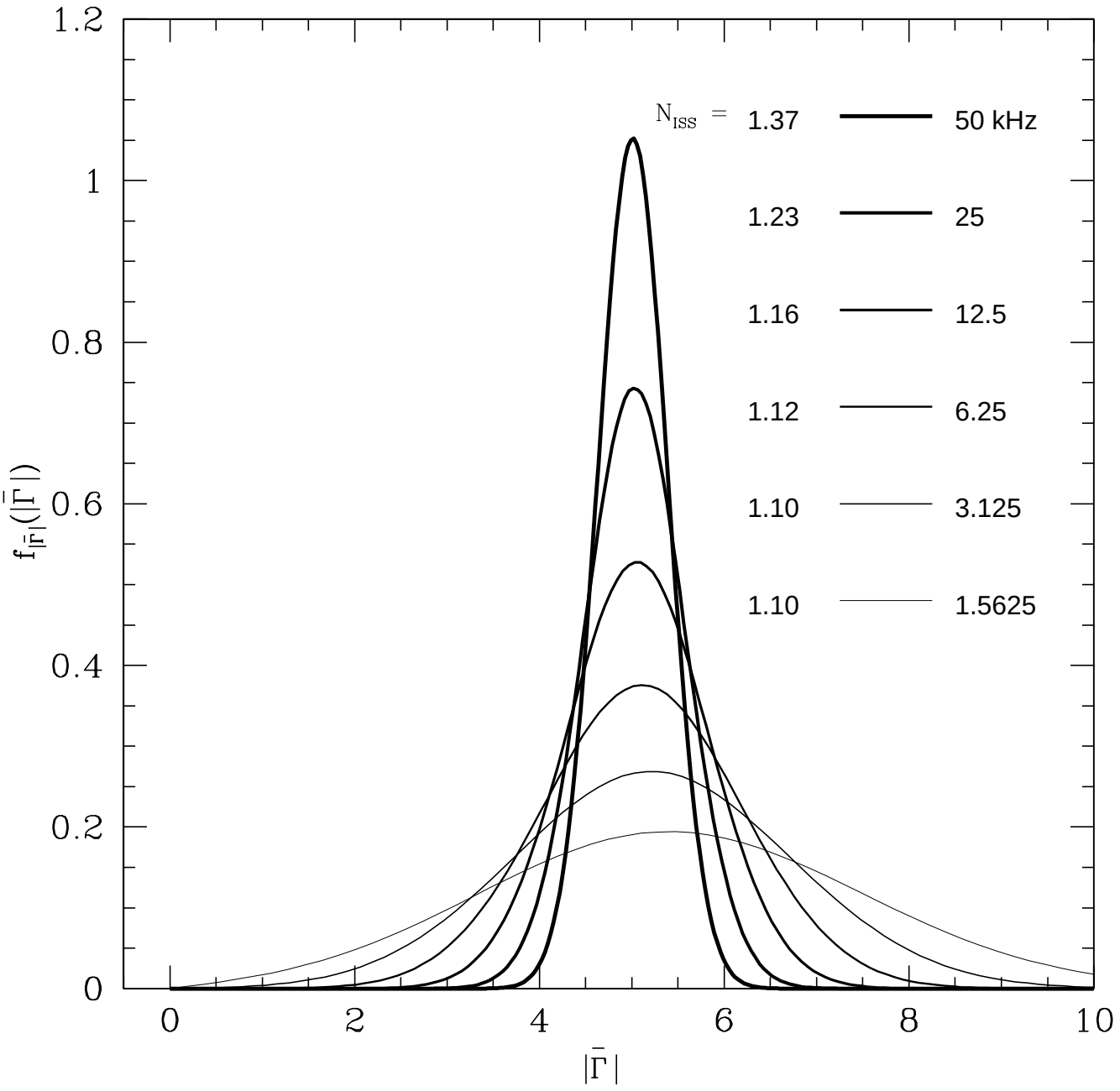

Fig. 9.— Same as Figure 8 except that ISS variations and the pulsar-noise term have been turned off by making the PDF's for G and X delta functions, $\delta(G-1)$ and $\delta(X)$, in Eq. C24-C25.

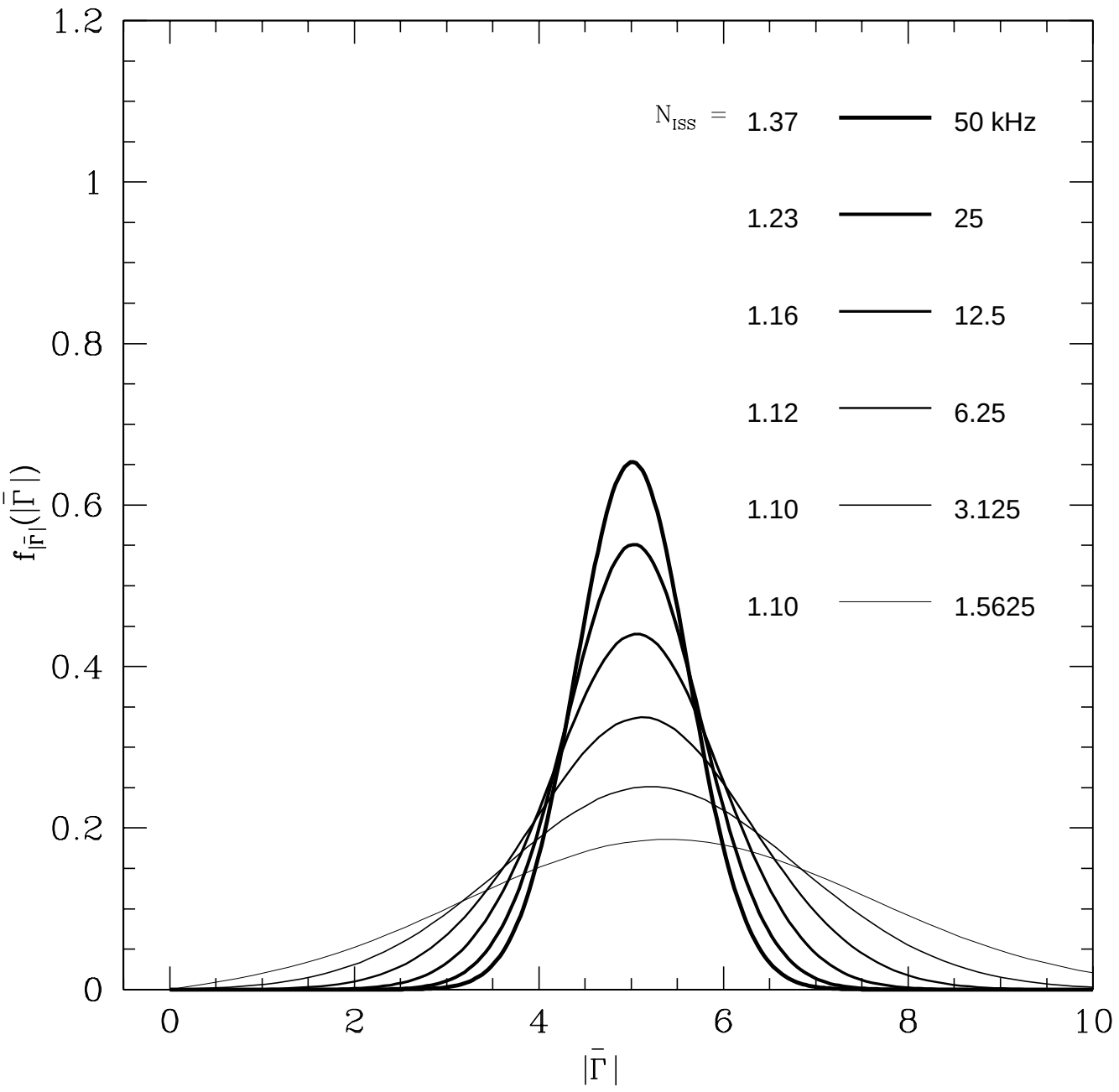

Fig. 10.— Same as Figures 8-9 except that here ISS variations are turned off but the pulsar noise variations X are turned on.

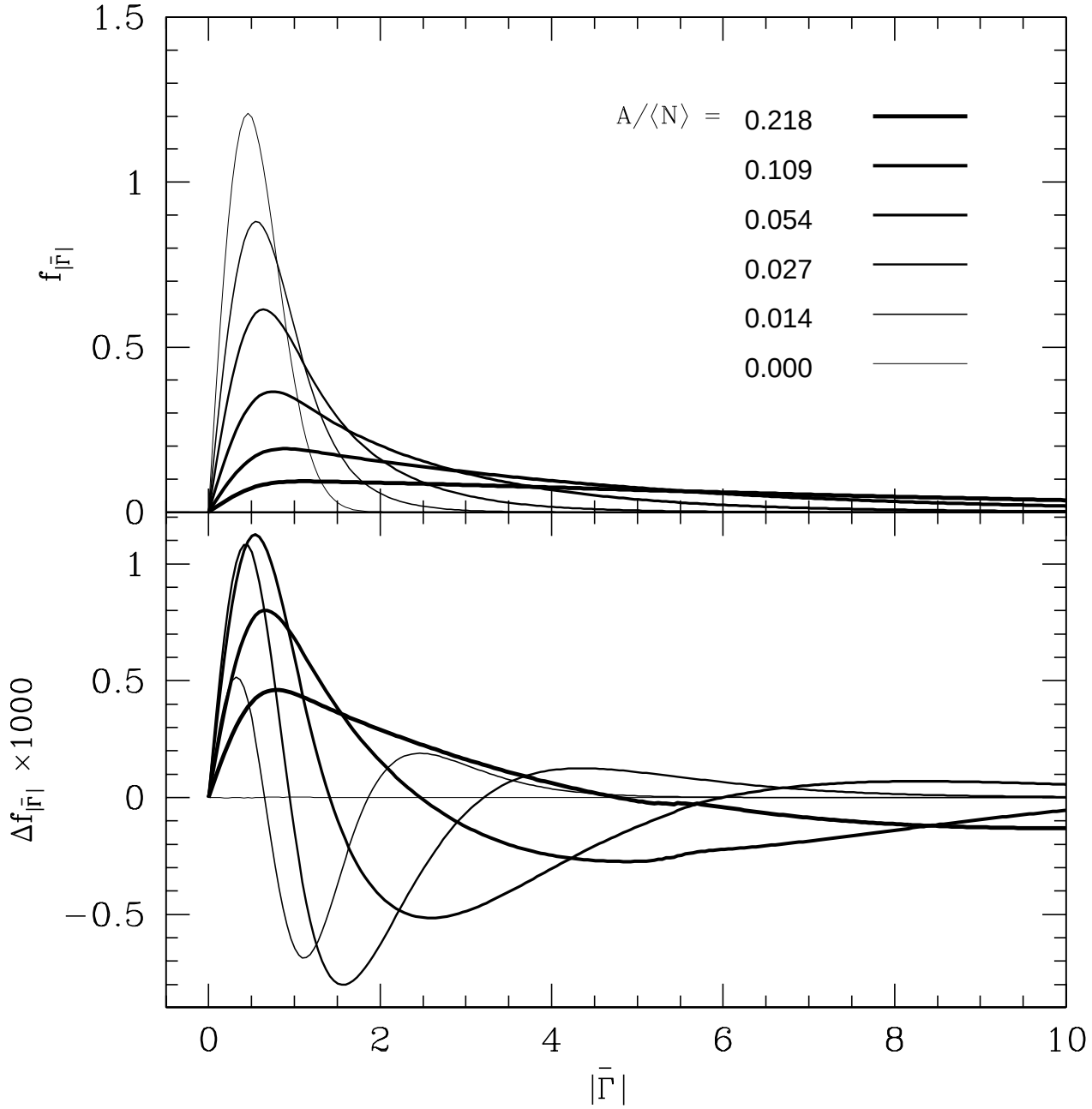

Fig. 11.— Top: Visibility PDF for different source strengths. The ratio of signal strength to mean noise strength is shown. The PDF's were calculated for $N_{\rm ISS} = 1.22$ and a bandwidth of 25 kHz. Bottom: Difference between the true PDF and the PDF while ignoring pulsar fluctuations. A positive value means that the true PDF exceeds the latter PDF.

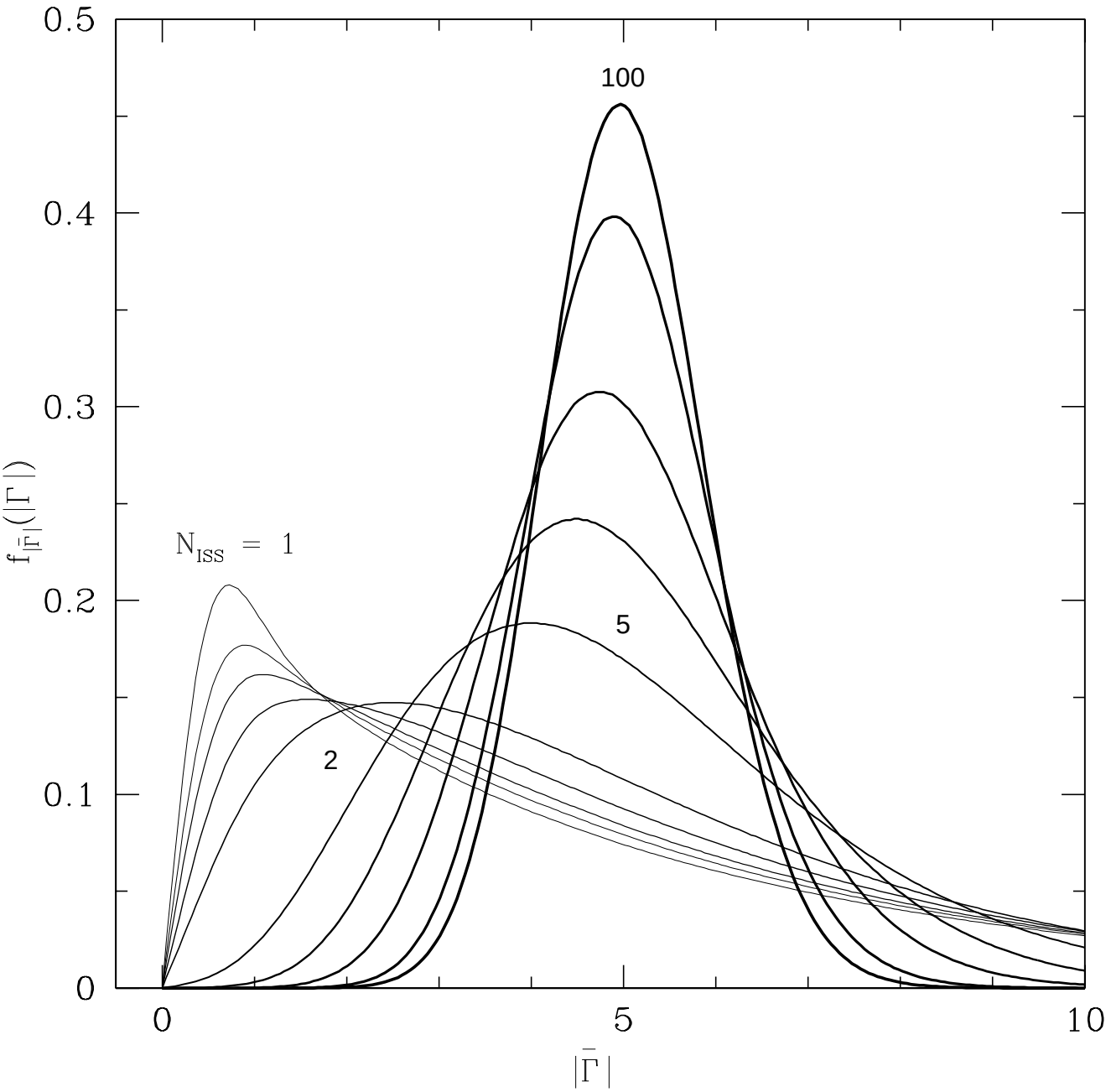

Fig. 12.— The PDF of the visibility magnitude when DISS is included with varying numbers of degrees of freedom, $2N_{\rm ISS}$, for $N_{\rm ISS} = 1, 1.125, 1.25, 1.5, 2, 5, 10, 20, 50$ and 100, with some values labelled. Results are shown for $\langle A \rangle / \sqrt{N_i N_j} = 0.14$. As $N_{\rm ISS} \rightarrow \infty$, the PDF tends toward a Gaussian function.